Alexander Mel'nikov, Sergey Mironov, and Alexander Buzdin

13 Interference phenomena in superconductor–ferromagnet hybrids

Abstract: The mismatch of Fermi surfaces for electrons with up and down spin orientation in ferromagnets leads to the oscillatory behavior of the Cooper pairs wavefunction. In the ballistic regime the Cooper pair phase accumulation depends on its trajectory and the exchange field along the trajectory. The critical current of the superconductor–ferromagnet–superconductor (SFS) Josephson junction results from the phase interference from different trajectories. We demonstrate how such an interference may produce a long-range singlet proximity effect. The additional spin–orbit interaction provides a mechanism for nonconventional Josephson junction formation, which may have an arbitrary phase difference in the ground state. As expected, scattering on the impurities weakens the interference effects. However, in the mesoscopic systems their presence may lead to new qualitative and observable effects.

13.1 Introduction

V. L. Ginzburg was the first to point out the antagonistic character of magnetism and superconductivity [1], by studying the orbital mechanism of interaction (via a vector potential $\boldsymbol{A}$) between them. Later it became clear that the singlet superconductivity is primarily destroyed by the exchange field h of the ferromagnet, making their coexistence impossible in bulk materials. This paramagnetic mechanism [2] is ineffective for the triplet Cooper pairs and now we know of four triplet ferromagnetic superconductors UGe_2, $URhGe$, $URhGe$ and UIr [3]. An overwhelming majority of superconductors are singlet ones and the interplay between magnetism and superconductivity is only possible in the superconductor–ferromagnet (SF) hybrid structures near the SF interface. During the last fifteen years an important progress has been achieved in experimental and theoretical studies of SF hybrids and a lot of interesting new phenomena was revealed (as reviews see [4–7]).

In the case of the proximity effect between superconductor and normal metal (N), the correlated electrons (Cooper pairs) penetrate into the normal metal at a mesoscopic length scale preserving their superconducting correlations and providing the superconducting current flow through SNS weak links [8]. The use of a ferromagnet

Alexander Mel'nikov, Institute for Physics of Microstructures RAS, 603950 Nizhny Novgorod, GSP-105, Russia, e-mail: melnikov@ipmras.ru
Sergey Mironov, Institute for Physics of Microstructures RAS, 603950 Nizhny Novgorod, GSP-105, Russia, e-mail: sermironov@rambler.ru
Alexander Buzdin, University Bordeaux, LOMA UMR-CNRS 5798, F-33405 Talence Cedex, France, e-mail: alexandre.bouzdine@u-bordeaux.fr

DOI 10.1515/9783110456806-014,

as a normal metal opens a way to manipulate the spin structure of the propagating Cooper pair. Both the internal magnetic field and exchange interaction in the ferromagnet lift a degeneracy with respect to spin orientation of the electrons. This leads to different de Broglie wavelengths of electrons at the Fermi surface for spin-up and spin-down orientation and produces a modulation of the Cooper pair wavefunction while propagating along the ferromagnet [4], similar to the Fulde–Ferrell–Larkin–Ovchinnikov state [9, 10]. As a result, an oscillatory damping of the superconducting wavefunction is known to appear when the ferromagnetic ordering occurs in a normal metal link connecting two S electrodes. This phenomenon provides the basis for the π-junction realization [11–13].

Considering the quantum mechanics of quasiparticle excitations this destructive effect of the exchange field can be viewed as a consequence of a phase difference $\gamma \sim L/\xi_h = 2Lh/\hbar v_F$ gained between the electron- and hole-like parts of the total wavefunction at the path of the length L [14, 15]. Here $\xi_h = \hbar v_F/2\,h$ is a characteristic length determined by the exchange field (v_F is the Fermi velocity). Both in the clean and dirty limits the measurable quantities should be calculated as superpositions of fast oscillating contributions $e^{i\gamma}$ from different trajectories and, thus, rapidly vanish with the increasing distance from the SF boundary.

As a result of this interference the critical current of SFS junction in the ballistic regime oscillates and decays with the thickness of the ferromagnetic layer d_f

$$I_c \sim \frac{\left|\sin\left(\frac{2d_f}{\xi_h}\right)\right|}{\left(\frac{2d_f}{\xi_h}\right)}\,. \tag{13.1}$$

The oscillatory behavior of the superconducting order parameter in ferromagnets produces the commensurability effects between the period of the order parameter oscillation (which is of the order of ξ_h) and the thickness of a F layer [16]. This results in the striking nonmonotonic superconducting transition temperature dependence on the F layer thickness in SF multilayers and bilayers [17].

In the diffusive regime the lengths of the trajectories increase dramatically and the decay of the superconducting correlation becomes exponential (and thus much faster) with a "dirty limit" characteristic length $\xi_f = \sqrt{\frac{D_f}{h}}$, where the diffusion coefficient in the F layer $D_f = \frac{1}{3}v_F l$ is determined by the electron mean free path l. This is related to the averaging of the fast oscillating contributions $e^{i\gamma}$ for many random trajectories created by scattering.

In the case of an inhomogeneous (noncollinear) exchange field distribution the so-called odd-frequency triplet pairing component in the anomalous Green functions is generated [5], which provides the mechanism for the long range proximity phenomena. The resulting dramatic increase in the range of superconducting correlations has been confirmed by the experiments on SFS Josephson junctions with a composite F layer containing a region with the noncollinear magnetic moments [18, 19].

In the present chapter we demonstrate that other possible mechanisms generating the long-range proximity effect exist due to the quantum interference phenomena. In Section 13.2 we study the Josephson junctions with composite F layer comprising the noncollinear regions in the ballistic regime. The interface between the noncollinear magnetic domains produces the magnetic scattering with the flip of the spins of the Cooper pair electrons. Therefore, the phases accumulated in different domains may have opposite signs and compensate each other. This phenomenon gives rise to the long-range Josephson current revealed by the first or second harmonics [20, 21] and opens a way to a simple control of the critical current of SFS junctions.

Another type of interference is provided by the nanowires, where the spin–orbit interaction competes with the orbital and exchange interactions and gives rise to the novel type of the Josephson "φ-junction" (with an arbitrary phase difference at the ground state) [22]. The physics of these interference phenomena is considered in Section 13.3.

Finally in Section 13.4 we consider the mesoscopic SFS structures and analyze in depth the averaging procedure in the presence of the potential scattering. It happens that the standard Usadel approach overlooks the mesoscopic sample-to-sample fluctuations of the Josephson current which are in fact long-range. Indeed, the destructive interference cannot play such a dramatic role when we calculate root-mean-square values due to partial phase gain compensation in squared quantities. This circumstance naturally explains the puzzling observation of the long-range SF proximity effect in the experiments [23–25], where no traces of a noncollinear magnetization were reported.

13.2 Josephson current through the composite ferromagnetic layer

The goal of this section is to show that the interference phenomena provide a possibility to cancel the particle–hole phase difference for a large group of quasiclassical trajectories due to either spatial or momentum dependence of the exchange field. Such a set of trajectories provides a long-range contribution to the Josephson current through a ferromagnetic system. We consider two generic examples which illustrate the above scenario of a long-range proximity effect: (i) Josephson transport through a pair of ferromagnetic layers with a stepwise exchange field distribution; (ii) Josephson transport through a nanowire with a specular electron reflection at the surface and exchange field varying with the changing quasiparticle momentum.

Josephson transport through a ferromagnetic bilayer

Let us start from the simplest model illustrating the origin of the quasiparticle interference suppression: Josephson junction containing two ferromagnetic layers of thicknesses d_1 and d_2, respectively (see Figure 13.1). Here we consider the limit of the short junction $d_1 + d_2 \ll \xi_s$, where ξ_s is the superconducting coherence length. The exchange fields $\boldsymbol{h}_1$ and $\boldsymbol{h}_2$ in the layers are rotated at the angle α. For the sake of simplicity we assume here the superconducting gap (exchange field) to vanish inside (outside) the F layer. The current–phase relation in the clean limit is known to be easily defined by the spectrum of the subgap Andreev states

$$\epsilon = \pm\Delta_0 \cos\left(\frac{\varphi + \gamma}{2}\right), \tag{13.2}$$

where Δ_0 is the temperature-dependent superconducting gap, φ is the Josephson phase difference, and $\gamma = \gamma_\sigma(\boldsymbol{n}_F)$ is the spin-dependent phase shift between the electron- and hole-like parts of the total wavefunction along the quasiclassical trajectory defined by the vector $\boldsymbol{n}_F$. Summing up over all trajectories we find the current–phase relation in the form:

$$I = \frac{1}{s_0}\int ds \int d\boldsymbol{n}_F \left[j(\varphi+\gamma) + j(\varphi-\gamma)\right](\boldsymbol{n}_F, \boldsymbol{n}), \tag{13.3}$$

where $s_0^{-1} = k_F/2\pi$ ($s_0^{-1} = (k_F/2\pi)^2$) for 2D (3D) junctions, $\boldsymbol{n}$ is the unit vector normal to the surface of the superconducting electrode, the integral $\int \ldots ds$ is taken over the junction cross-section, and

$$j(\varphi) = \frac{e\Delta_0}{2\hbar}\sin\frac{\varphi}{2}\tanh\left(\frac{\Delta_0\cos(\varphi/2)}{2T}\right) = \sum_{n\geq 1}\frac{j_n}{2}\sin(n\varphi). \tag{13.4}$$

is the current–phase relation for the junction of the same geometry and zero exchange field. The coefficients j_n in the above Fourier expansion read:

$$j_n = \frac{2eT}{\pi\hbar}\sum_{m=0}^{\infty}\int_0^{2\pi} d\chi \frac{\sin\chi\,\sin(n\chi)}{\mu_m + \cos\chi}, \tag{13.5}$$

where $\mu_m = 2\pi^2T^2(2m+1)^2/\Delta_0^2 + 1$.

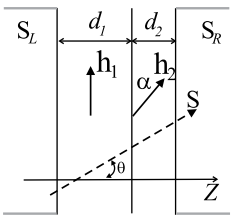

Fig. 13.1: Josephson junction containing two ferromagnetic layers. Linear quasiparticle trajectory is shown by the dashed line.

To find the phase gain γ for a certain of quasiclassical trajectory passing through the point $\boldsymbol{R}$ we should consider the Andreev-type equations:

$$-i\hbar v_{\mathrm{F}}\hat{\tau}_z\partial_s\hat{g} + \boldsymbol{h}(\boldsymbol{R}+s\boldsymbol{n}_F)\,\hat{\sigma}\hat{g} + \begin{pmatrix} 0 & \Delta(\boldsymbol{R}+s\boldsymbol{n}_F) \\ \Delta^*(\boldsymbol{R}+s\boldsymbol{n}_F) & 0 \end{pmatrix}\hat{g} = \epsilon\hat{g}\,, \tag{13.6}$$

where s is the coordinate along the trajectory, Δ is the gap function, $\hat{g} = (u, v)$, u and v are the electron- and hole-like parts of the quasiparticle wavefunction, and $\hat{\tau} = (\tau_x, \tau_y, \tau_z)$ is a vector of Pauli matrices in the electron–hole space. To find the phase γ induced by an arbitrary inhomogeneous exchange field $\boldsymbol{h}(\boldsymbol{r})$ we introduce a unitary transform (see also [15])

$$\hat{f} = \begin{pmatrix} f_u \\ f_v \end{pmatrix} = \hat{S}\,\hat{g} \qquad \hat{S} = \begin{pmatrix} \hat{S}_u & 0 \\ 0 & \hat{S}_v \end{pmatrix}, \tag{13.7}$$

with $\hat{S}_{u,v} = \alpha_{u,v} + i\beta_{u,v}\hat{\sigma}$ and exclude, thus, the exchange field term from the above equations inside the F layer. For this purpose we should solve the following set of equations

$$\hbar v_{\mathrm{F}}\partial_s\alpha_{u,v} = \mp\boldsymbol{h}\beta_{u,v}\,, \quad \hbar v_{\mathrm{F}}\partial_s\beta_{u,v} = \pm\alpha_{u,v}\boldsymbol{h} \pm [\boldsymbol{h}, \beta_{u,v}]\,, \tag{13.8}$$

with the boundary conditions

$$\alpha_{u,v}(0) = 1, \quad \beta_{u,v}(0) = 0\,,$$

at the left superconducting electrode (at $s = s_L$). The operator modifying the order parameter in the right half–space takes the form:

$$\hat{S}_u\hat{S}_v^{+} = \alpha_u\alpha_v + (\beta_u\beta_v) + i\hat{\sigma}\left(\alpha_v\beta_u - \alpha_u\beta_v + [\beta_u, \beta_v]\right)\,, \tag{13.9}$$

where the values $\alpha_{u,v}$ and β_{uv} should be taken at the right superconducting electrode (at $s = s_R$). Choosing an appropriate direction of the spin quantization axis in the above expression (i.e., along the vector $\alpha_v\beta_u - \alpha_u\beta_v + [\beta_u, \beta_v]$) we find the final expression for an additional order parameter phase γ induced by the exchange field:

$$e^{i\gamma} = \alpha_u\alpha_v + (\beta_u\beta_v) \pm i\left|\alpha_v\beta_u - \alpha_u\beta_v + [\beta_u, \beta_v]\right|\,. \tag{13.10}$$

The phase γ can be conveniently determined from the Eilenberger-type equations if we introduce the singlet and triplet parts of the anomalous quasiclassical Green function $f = f_s + \mathbf{f}_t\hat{\sigma}$ according to the expressions

$$f_s = \cos\gamma = \alpha_u\alpha_v + (\beta_u\beta_v) \tag{13.11}$$

$$\mathbf{f}_t = i\left(\alpha_u\beta_v - \alpha_v\beta_u + [\beta_u, \beta_v]\right)\,. \tag{13.12}$$

Using Equations (13.8) we find the linearized Eilenberger equations written for zero Matsubara frequencies

$$-i\hbar v_{\mathrm{F}}\partial_s f_s + 2\mathbf{h}\mathbf{f}_t = 0\,, \tag{13.13}$$

$$-i\hbar v_{\mathrm{F}}\partial_s\mathbf{f}_t + 2f_s\mathbf{h} = 0\,. \tag{13.14}$$

So, the phase gain γ along the trajectory in SFS constriction is determined by the singlet part of the anomalous quasiclassical Green function $f_s(s = s_R) = \cos\gamma$ taken at the right superconducting electrode.

Finally, the current–phase relation reads:

$$I = \sum_n I_n = \sum_n a_n \sin n\varphi \frac{\langle (\boldsymbol{n}, \boldsymbol{n}_F) \cos n\gamma \rangle}{\langle (\boldsymbol{n}, \boldsymbol{n}_F) \rangle} , \tag{13.15}$$

where $\boldsymbol{n}$ is the unit vector normal to the junction plane, $\boldsymbol{n}_F$ is the unit vector along the trajectory, and

$$a_n = j_n N = j_n \frac{1}{s_0} \int ds \int d\boldsymbol{n}_F (\boldsymbol{n}_F, \boldsymbol{n}) ,$$

are the coefficients of the Fourier expansion for the current–phase relation $I_{\mathrm{SNS}}(\varphi)$ for zero exchange field, i.e., for superconductor–normal metal junction of the same geometry. The angular brackets denote the averaging over different quasiclassical trajectories. The first two coefficients in this expansion take the form:

$$a_n = \frac{4eT}{\hbar} N(-1)^{n-1} \sum_{m=0}^{\infty} \left(\mu_m - \sqrt{\mu_m^2 - 1} \right)^n , \ n = 1, 2 , \tag{13.16}$$

where $\mu_m = 2\pi^2 T^2 (2m+1)^2 / \Delta_0^2 + 1$, Δ_0 is the temperature-dependent superconducting gap, $N = s_0^{-1} \int ds \int d\boldsymbol{n}_F (\boldsymbol{n}_F, \boldsymbol{n})$, and the integral $\int \ldots ds$ is taken over the junction cross-section. The factor N is determined by the number of transverse modes in the junction: $N \sim S/s_0$, where S is the junction cross-section area.

Solving the above Eilenberger-type equations for the particular bilayer geometry we find:

$$\cos\gamma = \cos^2 \frac{\alpha}{2} \cos\left(\frac{d_1 + d_2}{\xi_h \cos\theta} \right) + \sin^2 \frac{\alpha}{2} \cos\left(\frac{d_1 - d_2}{\xi_h \cos\theta} \right) , \tag{13.17}$$

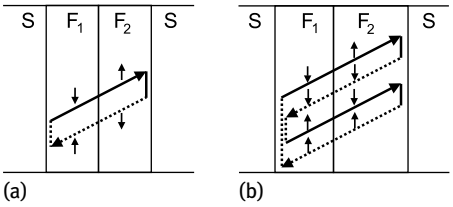

Fig. 13.2: The examples of the closed electron (straight lines) and hole (dashed lines) trajectories for the Andreev reflection which have no phase accumulation. For such trajectories averaging over the angles does not lead to destructive interference. The vertical arrows indicate the spin direction for each part of the trajectory. (a) Possible trajectory which provides the phase compensation for equal thicknesses $d_1 = d_2$ and give rise to the long-range first harmonic of the current–phase relation. (b) Possible trajectory which provides the phase compensation for arbitrary thicknesses of the F_1 and F_2 layers and gives rise to the long-range second harmonic of the current–phase relation.

where $\cos\theta = (\boldsymbol{n}, \boldsymbol{n}_F)$. This expression allows us to write the first harmonic in the current–phase relation in the form:

$$I_1 = \left[\cos^2\frac{\alpha}{2} I_{c1}\left(\frac{d_1 + d_2}{\xi_h}\right) + \sin^2\frac{\alpha}{2} I_{c1}\left(\frac{d_1 - d_2}{\xi_h}\right)\right]\sin\varphi\,, \tag{13.18}$$

where $I_{c1}(d/\xi_h)$ is the critical current of the first harmonic in a SFS junction with a homogeneous exchange field h. The interference effects discussed in the introduction result in the power decay of the critical current I_{c1} vs the F layer thickness d: $I_{c1} \propto d^{-1/2}$ for a 2D junction [27] and $I_{c1} \propto d^{-1}$ for a 3D junction [11]. Taking the symmetric case $d_1 = d_2$ (see Figure 13.2a) we immediately get a long-range contribution to the Josephson current

$$\delta I_{c1} = \sin^2\frac{\alpha}{2} I_{c1}(0)\sin\varphi\,, \tag{13.19}$$

which does not decay with the increasing distance between the S electrodes. It is important to note that this contribution *does not vanish for an arbitrary nonzero angle* between the magnetic moments in the F layers.

Long-range behavior can be observed for a second harmonic in the current–phase relation as well. Indeed, calculating the average $\langle(\boldsymbol{n}, \boldsymbol{n}_F)\cos 2\gamma\rangle$ we find a nonvanishing long-range supercurrent contribution even for $d_1 \neq d_2$ (see Figure 13.2b):

$$\delta I_{c2} = \frac{a_2 \sin^2\alpha}{2}\sin 2\varphi\,. \tag{13.20}$$

Note, that the emergence of a long-range proximity effect for high harmonics in Josephson relation is in a good agreement with recent theoretical findings in [28, 29] (see Figure 13.2b and the similar figure in [28]).

The long range proximity via controlled magnetic scattering

As we have noted the short range of the proximity effect in the ferromagnets is due to the Cooper pairs phase accumulation over its trajectory. The Josephson junction with two noncollinear ferromagnetic layers, considered above provides the mechanism to avoid this. Another way to compensate such phase accumulation is to introduce the magnetic scatterer at the middle of the path of the Cooper pair [21]. Indeed the spin-flip scattering changes the spin arrangement of a pair: if initially the pair have a nonzero

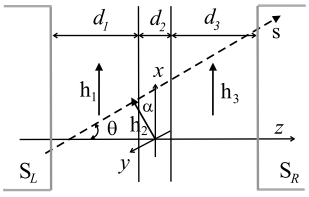

Fig. 13.3: SFS Josephson junction containing three ferromagnetic layers (domains) with a stepwise profile of the exchange field. Linear quasiparticle trajectory is shown by the dashed line.

total momentum $\hbar\boldsymbol{q} = \hbar\boldsymbol{k}_\uparrow - \hbar\boldsymbol{k}_\downarrow$ ($|\boldsymbol{q}| \sim 1/\xi_h$) then after the spins flip the new total momentum of the Cooper pair $\hbar\boldsymbol{q}'$ is reversed $\hbar\boldsymbol{q}' = -\hbar\boldsymbol{q}$. Let us consider the Josephson transport through a ballistic SFS junction containing three ferromagnetic layers (domains) with a stepwise profile of the exchange field

$$h(z) = \begin{cases} h\boldsymbol{x}_0, & \text{in domains} \quad d_1, d_3 \\ h\left(\boldsymbol{x}_0 \cos\alpha + \boldsymbol{y}_0 \sin\alpha\right), & \text{in domain} \quad d_2\,, \end{cases} \tag{13.21}$$

where α is the angle of the exchange field rotation in the central domain d_2 (see Figure 13.3). At a symmetric position of the scatterer ($d_1 \simeq d_3$) the total phase gain $\gamma \sim (d_1 - d_3)/\xi_h$ for a singlet Cooper pair should be cancelled out and the long-range singlet superconducting proximity in SFS link becomes possible. So the introduction of the additional noncollinear ferromagnetic layer may strongly increase the critical current of SFS junction!

To calculate the current–phase relation for the junction Figure 13.3 we may start with a general formula (13.15) and calculate the phase gain $\gamma(\theta)$ along a trajectory $\boldsymbol{s} = s\,\boldsymbol{n}_F$ (see Figure 13.3), which is $\cos\gamma = f_s(s_R)$.

To consider the Josephson transport through ferromagnetic layer with an arbitrary noncollinear distribution of the magnetizations $\boldsymbol{M}$ and the exchange field $\boldsymbol{h}$ it is convenient to utilize the transfer matrix formalism [21]. For this, we need to solve Equations (13.13) and (13.14) for the case when the quantization axis is taken arbitrarily in the ferromagnetic layer of a thickness $d_i = z_i - z_{i-1}$. We assume that a quasiclassical trajectory $\boldsymbol{s}$ is characterized by a given angle θ with respect to the z-axis and exchange field $\boldsymbol{h} = h\left(\boldsymbol{x}_0 \cos\alpha_i + \boldsymbol{y}_0 \sin\alpha_i\right)$ lie in the plane $(x,\ y)$, as shown in Figure 13.3. The triplet part $\boldsymbol{f}_t$ consists of two nonzero components and can be written as $\boldsymbol{f}_t = f_{tx}\boldsymbol{x}_0 + f_{ty}\boldsymbol{y}_0$. Defining the transfer matrix $\hat{T}_{\alpha_i}(d_i, \theta)$ that relates the components of the Green function $\hat{f}(s) = \{f_s(s),\ f_{tx}(s),\ f_{ty}(s)\}$ at the left ($s = s_{i-1} = z_{i-1}/\cos\theta$) and right ($s = s_i = z_i/\cos\theta$) boundaries of the F layer,

$$\hat{f}(s_i) = \hat{T}_{\alpha_i}(d_i, \theta)\hat{f}(s_{i-1})\,, \tag{13.22}$$

we get the following expression:

$$\hat{T}_{\alpha_i}(d_i, \theta) = \begin{pmatrix} \cos(qs_{d_i}) & -i\cos\alpha_i \sin(qs_{d_i}) & -i\sin\alpha_i \sin(qs_{d_i}) \\ -i\cos\alpha_i \sin(qs_{d_i}) & \sin^2\alpha_i + \cos^2\alpha_i \cos(qs_{d_i}) & \sin\alpha_i \cos\alpha_i \left(\cos(qs_{d_i}) - 1\right) \\ -i\sin\alpha_i \sin(qs_{d_i}) & \sin\alpha_i \cos\alpha \left(\cos(qs_{d_i}) - 1\right) & \cos^2\alpha_i + \sin^2\alpha_i \cos(qs_{d_i}) \end{pmatrix}, \tag{13.23}$$

where $q \equiv 1/\xi_h = 2\,\mathrm{h}/\hbar v_\mathrm{F}$ and $s_{d_i} = d_i/\cos\theta$.

Solving Equations (13.13) and (13.14) by the transfer matrix method for the stepwise profile of the exchange field (13.21), the anomalous quasiclassical Green function $\hat{f}(s_R) = \{f_s(s_R),\ f_{tx}(s_R),\ f_{ty}(s_R)\}$ at the right superconducting electrode ($s = s_R =$

$d/\cos\theta$) can be easily expressed via the boundary conditions $\hat{f}(0) = (1, 0, 0)$ at the left superconducting electrode ($s = 0$) as follows:

$$\hat{f}(s_R) = \hat{T}_0(d_3, \theta)\, \hat{T}_\alpha(d_2, \theta)\, \hat{T}_0(d_1, \theta)\hat{f}(0)\,, \tag{13.24}$$

where $d = d_1 + d_2 + d_3$ is the total thickness of the ferromagnetic barrier, and the transfer matrix $\hat{T}_\alpha(d_i, \theta)$ is determined by the expression (13.23). As a result:

$$\cos\gamma = \cos\delta_2 \cos(\delta_1 + \delta_3) - \cos\alpha \sin\delta_2 \sin(\delta_1 + \delta_3) \tag{13.25}$$

$$- \sin^2\alpha\, \sin\delta_1 \sin\delta_3 (1 - \cos\delta_2)\,, \tag{13.26}$$

where $\cos\theta = (\boldsymbol{n}, \boldsymbol{n}_F)$ and $\delta_i = d_i/\xi_h \cos\theta$ ($i = 1, 2, 3$). Averaging the expression (13.25) over the trajectory direction θ and neglecting the terms proportional to $\xi_h/d \ll 1$, which decrease just as for the case of homogeneous ballistic 3D SFS junction, one arrives at the following long-range (LR) contribution:

$$(\cos\gamma)^{LR} = -\frac{1}{2} \sin^2\alpha (1 - \cos\delta_2)\, \cos 2\delta_z\,, \tag{13.27}$$

where $\delta_z = z_0/\xi_h \cos\theta$ and $z_0 = (d_1 - d_3)/2$ is the shift of the central domain with respect to the weak link center.

For a thin central domain $d_2 \ll \xi_h$ in the center ($z_0 = 0$) one can easily estimate from (13.27) the critical current of the SFS junction

$$\max\{I^{LR}\} \approx \frac{I_0}{2} \sin^2\alpha \left(\frac{d_2}{\xi_h}\right)^2 \ln\frac{\xi_h}{d_2}\,, \tag{13.28}$$

where $I_0 = (eT_cN/8\hbar)(\Delta/T_c)^2$ is the critical current of the SNS junction for zero exchange field ($\gamma = 0$). Figure 13.4a shows the dependence of the maximal Josephson current $I_c^{LR} = a_1 T_1^{LR}$ on the thickness d_2 of the 90^o domain ($\alpha = \pi/2$) for different positions of the domain with respect to the weak link center. The amplitude of I^{LR} oscillates with varying the thickness of the central domain d_2, and has the first maximum at $d_2 \simeq 2.5\xi_h$. Naturally, when the central domain disappears ($d_2 \to 0$), the long-range effect vanishes. We see that the long-range critical current reaches the maximum at $\alpha = \pi/2$ and grows with the increase of d_2 up to $d_2 \sim \xi_h$. The numerical calculations show that it is maximum for $d_2 \simeq 2.5\,\xi_h$ and may reach $\sim 0.7 I_0$.

Figure 13.4b shows the dependences of the maximal Josephson current I_c on the position of the central domain z_0 for different values of the rotation angle α. We may see that the critical current is quite sensitive to the position of the central domain and the first zero of I_1 occurs already at $z_0 \simeq 0.5\xi_h$.

The transfer matrix formalism can be easily generalized for a layered ferromagnetic barrier with an arbitrary noncollinear distribution of the exchange field and qualitatively the long range singlet proximity effect occurs to be quite robust [21]. In contrast to the widely discussed triplet long-range proximity effect where the thin lateral F-layers are needed [30], here the required geometry is somewhere complimentary with the thin central layer.

The interesting property of the discussed system is that it provides a direct mechanism of the coupling between supercurrent and magnetic moment, similar to the situation discussed in [31]. Since the long-range critical current I_c^{LR} depends on the profile of the magnetization, the superconducting current acts as a direct driving force on the magnetic moment and can change its orientation. Inversely, the precession of the magnetic moment shall modulate the critical current.

Josephson current through a ferromagnetic wire

We now consider a more complicated example of the interference phase suppression in a ferromagnetic wire where the quasiclassical trajectories of electrons and holes experience multiple specular reflections from the wire surface (see Figure 13.5a). The particular geometry shown in Figure 13.5a can be considered as a rough model for experiments on Co nanowires [25]. For simplicity we restrict ourselves to the case of a short 2D junction with $L \ll \xi_S$.

Taking into account the spin–orbit interaction inside the ferromagnet we obtain the exchange part of the effective Hamiltonian for the band electrons depending on the

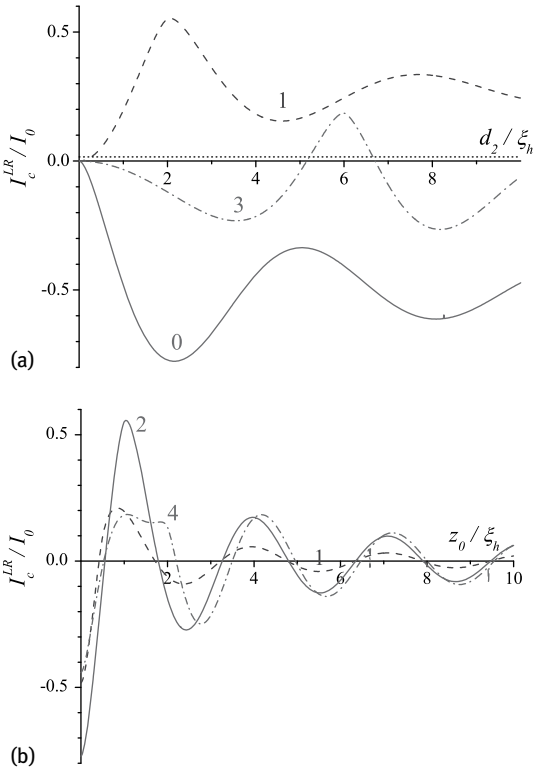

Fig. 13.4: (a) The dependence of I_c^{LR} on the thickness d_2 of the 90^o domain ($\alpha = \pi/2$) for different values of the shift of the domain z_0: $z_0 = 0$ (solid line); $z_0 = \xi_h$ (dashed line); $z_0 = 3\xi_h$ (dash-dotted line). Dotted line shows the value of $I_c = \max\{I_1\}$ in absence of domain d_2. (b) The dependence of maximal Josephson current I_c^{LR} on the shift of the central domain z_0 for different values of the d_2: $d_2 = \xi_h$ (dashed line); $d_2 = 2\xi_h$ (solid line); $d_2 = 4\xi_h$ (dash-dotted line). We have set $T = 0.9T_c$; $d = 50\xi_h$ [$I_0 = (eT_cN/8\hbar)(\Delta/T_c)^2$].

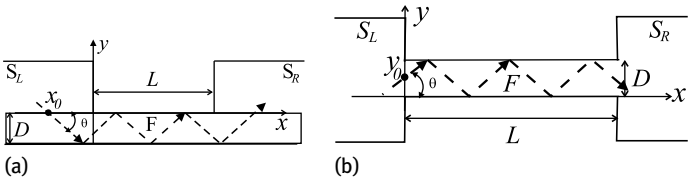

Fig. 13.5: Josephson transport through a nanowire in the overlap (a) and edge (b) geometries. The quasiparticle trajectories are shown by the dashed lines.

quasimomentum ($\boldsymbol{k}$) orientation [32]:

$$\hat{H}_{\rm ex} = \sum_{ij} \beta_{ij}(\boldsymbol{k}) h_{0i} \sigma_j = \boldsymbol{h}(\boldsymbol{k})\hat{\sigma} \ ,$$

where $\boldsymbol{h}_0$ is a pseudovector determined by the ferromagnetic moment. Assuming the absence of the system anisotropy described by a polar vector we find the simplest form of the resulting exchange field: $\boldsymbol{h} = \boldsymbol{h}_0 + \beta_{\rm so} k_{\rm F}^{-2}(\boldsymbol{h}_0, \boldsymbol{k})\boldsymbol{k}$, where $\beta_{\rm so}$ is a constant determined by the spin–orbit interaction, and $k_{\rm F}$ is the Fermi momentum.

The exchange field along the quasiparticle trajectory experiencing the reflection at the wire surface should change its direction. Thus, we obtain the problem described by Equations (13.13), (13.14) with a periodic exchange field along the trajectory characterized by a given angle θ and a certain starting point at the superconductor surface. The same equations for each trajectory can be of course derived for a periodic domain structure. Let us consider first the problem of calculating the band spectrum $\epsilon(k)$ in the field $\boldsymbol{h}$ varying with the period $2D/\sin\theta$:

$$-i\hbar v_{\rm F}\partial_s f_s + 2\boldsymbol{h}\boldsymbol{f}_t = \epsilon(k) f_s \ , \tag{13.29}$$

$$-i\hbar v_{\rm F}\partial_s \boldsymbol{f}_t + 2 f_s \boldsymbol{h} = \epsilon(k)\boldsymbol{f}_t \ . \tag{13.30}$$

The solution can be written in the Bloch form:

$$\begin{pmatrix} f_s \\ \boldsymbol{f}_t \end{pmatrix} = e^{iks} \begin{pmatrix} f_{sk} \\ \boldsymbol{f}_{tk} \end{pmatrix} \ ,$$

where $f_{sk}(s + 2D/\sin\theta) = f_{sk}(s)$ and $\boldsymbol{f}_{tk}(s + 2D/\sin\theta) = \boldsymbol{f}_{tk}(s)$. Provided that this solution corresponds to the energy branch $\epsilon_\sigma(k)$ another solution $(f_s^*, -\boldsymbol{f}_t^*)$ corresponding to the energy $-\epsilon_\sigma(k)$ exists. The latter solution corresponds also to the energy $\epsilon_{\tilde{\sigma}}(-k)$ and, thus, we obtain the following symmetry property of the band spectrum: $\epsilon_{\tilde{\sigma}}(-k) = -\epsilon_\sigma(k)$, where the indices σ and $\tilde{\sigma}$ denote different branch numbers. The full set of energy branches can be split in such pairs provided the number of branches is even. For an odd number of branches there is always one branch which does not have a partner. For this branch we obtain $\epsilon_\sigma(-k) = -\epsilon_\sigma(k)$ and, thus, this spectrum branch crosses the zero energy level at $k = 0$: $\epsilon_\sigma(0) = 0$. The corresponding phase gain γ appears to vanish for trajectories containing an integer number of periods shown in Figure 13.5a and, therefore, the solution with $k = 0$ and $\epsilon = 0$ provides a long-range

contribution to the supercurrent. Note that this zero energy state is somewhat similar to the Majorana midgap state (see [33, 34] for review).

We choose the field $\boldsymbol{h}_0$ to be directed along the wire axis x and obtain the exchange field in the form: $\boldsymbol{h} = \boldsymbol{x}_0 h_x + \boldsymbol{y}_0 h_y(s)$, where $h_x(\theta) \simeq h_0$ is constant along the trajectory and $h_y(s)$ is a periodic function with zero average. In the interval $-D/\sin\theta < s < D/\sin\theta$ the h_y field component is defined by the expression $h_y = \beta_{so} h_0 \sin\theta\cos\theta \ \mathrm{sign}\, s$. Introducing the Fourier expansions

$$h_y = \sum_q H_q \mathrm{e}^{iqs}, \quad H_q = -i\tilde{h}\frac{2\sin\theta}{Dq},$$
$$f_{s,tx,ty} = \mathrm{e}^{iks}\sum_q F_{s,x,y}(k+q)\mathrm{e}^{iqs},$$

we rewrite Equations (13.29) and (13.30) in the form:

$$(\hbar v_F(k+q) - \epsilon)F_s(k+q) + 2h_x F_x(k+q) + 2\sum_{\tilde{q}} H_{q-\tilde{q}} F_y(k+\tilde{q}) = 0, \tag{13.31}$$

$$(\hbar v_F(k+q) - \epsilon)F_x(k+q) + 2h_x F_s(k+q) = 0, \tag{13.32}$$

$$(\hbar v_F(k+q) - \epsilon)F_y(k+q) + 2\sum_{\tilde{q}} H_{q-\tilde{q}} F_s(k+\tilde{q}) = 0. \tag{13.33}$$

Here $q, \tilde{q} = q_m = \pi(2m+1)\sin\theta/D$, m is an integer, and $\tilde{h} = \beta_{so} h_0 \sin\theta\cos\theta$.

To get the solution for a small periodic field h_y we use a perturbative approach similar to the nearly free electron approximation in the band theory of solids and restrict the number of interacting Fourier harmonics in the expansions. For this purpose it is instructive to consider the limit of zero periodic potential h_y and separate three solutions: (i) the solution $(F_s, F_x, F_y) = (0, 0, 1)\delta_{q-p}$ corresponding to the energy $\epsilon_0 = \hbar v_F(k+p)$ (ii) the solution $(F_s, F_x, F_y) = (1, 1, 0)\delta_{q-p_+}$ corresponding to the energy $\epsilon_+ = \hbar v_F(k+p_+) + 2h_x$, and (iii) the solution $(F_s, F_x, F_y) = (1, -1, 0)\delta_{q-p_-}$ corresponding to the energy $\epsilon_- = \hbar v_F(k+p_-) - 2h_x$. Here p and $p_\pm$ are arbitrary reciprocal lattice vectors. The above modes should strongly interact provided that the resonant condition $\epsilon_0 = \epsilon_+ = \epsilon_-$ is fulfilled. Such resonance is possible when the value $2h_x/\hbar v_F$ equals a certain reciprocal lattice vector q_m. Close to such Bragg-type resonance we see that the dominant harmonics correspond to the following choice of reciprocal lattice vectors: $p = 0$, $p_\pm = \mp q_m$. Writing the solution as a superposition of these three harmonics we find renormalized spectral branches $\epsilon_0 = \hbar v_F k$, $\epsilon_\pm = \hbar v_F k \pm \sqrt{(\hbar v_F q_m - 2h_x)^2 + 8|H_{q_m}|^2}$ and relative eigenfunctions. Applying now the boundary conditions at $s = 0$ for the superposition of the above eigenfunctions we find the amplitude of the singlet component corresponding to the energy branch ϵ_0 and $k = 0$:

$$f_{sm} = \frac{8|H_{q_m}|^2\cos(q_m s)}{(\hbar v_F q_m - 2h_x)^2 + 8|H_{q_m}|^2}.$$

At the surface of a right superconducting electrode we should take the coordinate s to be equal to the integer number of periods. We also need to sum up the above resonant expressions over all Fourier harmonics of the periodic potential:

$$f_s(s = s_R) = \sum_{m=0}^{\infty} \frac{8|H_{q_m}|^2}{(\hbar v_F q_m - 2h_x)^2 + 8|H_{q_m}|^2} .$$

The precision of such resonant-type expression has also been confirmed by the numerical solution of Equations (13.29) and (13.30), carried out using the transfer matrix method. Note, that we omit here the contribution from the solutions corresponding to the branches $\epsilon_{\pm}$: these functions correspond to a nonzero quasimomentum and, thus, should gain a finite phase factor along the trajectory length. During averaging over different trajectories this phase factor causes the suppression of the resulting supercurrent contribution with the increase of the wire length L.

The starting point of the trajectory varies in the interval $\Delta x = 2D/\tan\theta$ and, as a consequence, the long-range first harmonic in current–phase relation takes the form:

$$I_1 = a_1 \sin\varphi \int_0^{\pi/2} d\theta \cos\theta f_s(s_R) .$$

Assuming narrow resonances we approximate them by the delta-functions and obtain:

$$I_1 = a_1 \sin\varphi \sum_m \frac{\sqrt{2}\pi\hbar v_F \tilde{h}(\theta_m)}{h_x^2 D} \sin^2\theta_m ,$$

where $\sin\theta_m = 2h_x D/\pi\hbar v_F(2m+1)$. In the limit $D \gg \hbar v_F/2h_x$ one can replace the sum over m by the integral:

$$I_1 \simeq a_1\sqrt{2} \int_0^{\pi/2} d\theta \frac{\tilde{h}(\theta)}{h_x(\theta)} \cos\theta \sin\varphi \simeq a_1 \frac{\sqrt{2}}{3} \beta_{s0} \sin\varphi .$$

Certainly, the above long-range effect in the first harmonic is rather sensitive to the system geometry and possible disorder. Taking, e.g., the system sketched in Figure 13.5b we will not obtain the full cancellation of the phase γ because the trajectories in this case do not contain integer number of exchange field modulation periods. The breakdown of the exchange field periodicity due to nonspecular quasiparticle reflection at the wire surface mixes the solutions with $\epsilon = 0$ and different quasimomenta k and, thus, should also prevent the full cancellation of the phase γ. However, similarly to the case of the bilayer we expect the long-range effect to be still possible for higher harmonics. We apply the above perturbative procedure for the calculation of the full f_s function for the geometry shown in Figure 13.5b.

The second harmonic in the current–phase relation reads

$$I_2 = a_2 \sin 2\varphi \int_0^{\pi/2} d\theta \cos\theta \left(2\langle f_s^2(s_R)\rangle_{y_0} - 1 \right) , \tag{13.34}$$

where $\langle \ldots \rangle_{y_0} = (1/D) \int_0^D \ldots dy_0$ denotes averaging over the starting point of the trajectory y_0 (see Figure 13.5b). Keeping only the terms linear in the small $|H_{q_m}|$ amplitude we get the following expression for the long-range part of the second harmonic I_2:

$$I_2 = a_2 \sin 2\varphi \sum_m \frac{\sqrt{2}\pi\hbar v_F \tilde{h}(\theta_m)}{h_x^2 D} \sin^2 \theta_m \simeq a_2 \frac{\sqrt{2}}{3} \beta_{s0} \sin 2\varphi \ .$$

We emphasize that the second harmonic of the Josephson current in both examples described above is negative because of the condition $a_2 < 0$.

Note that the absence of the decay of the single-channel critical current was pointed out in [35] as a possible source of the long-range proximity effect in Co nanowires. However the averaging of the phase gain for different modes strongly decreases the critical current. In contrast the results presented in this section demonstrate that in the ballistic regime the spin-orbit interaction generates the noncollinear exchange field which produces the long-range Josephson current. This conclusion is always true for the second harmonic in the current–phase relation and for some geometries it may be also valid for the first harmonic. Therefore our findings provide a natural explanation of the recent experiments with Co nanowire [25]. To discriminate between two proposed mechanisms of the long-range effect, the studies of higher harmonics in Josephson current–phase relations could be of major importance. Also it should be interesting to verify with experiment the predicted simple angular dependence (13.19) of the critical current in SFS junctions with composite interlayer.

13.3 Interference phenomena in nanowires

The systems with a few conductive channels reveal unusual interference phenomena arising from the interplay between the spin–orbit, Zeeman and orbital interactions. The experimental realization of such systems is based, e.g., on the localized electronic states appearing at the surface of topological insulators [36], at the edges of graphene nanoribbons [37], and InAs, InSb and Bi nanowires [38–41]. The physics of the Josephson transport through these states appears to be extremely rich since they combine several unique properties which are not available simultaneously in conventional SFS junctions: (i) large Fermi wavelength $\lambda_F \sim 50$ nm, which makes the transport through the edge states nearly one-dimensional [42]; (ii) large g-factor $\sim 10^2$ for certain directions of magnetic field $\boldsymbol{H}$ [43], which makes the effect of the Zeeman spin-splitting significant even without the ferromagnetic order; (iii) strong Rashba spin–orbit coupling with the energy comparable with the Fermi energy [44, 45].

In this section we discuss two main effects arising in such Josephson systems: multiperiodic magnetic oscillations of the critical current I_c [22, 46] and the formation of the φ_0-junction with the arbitrary phase difference φ_0 in the ground state [22, 31]. The oscillations of I_c originate from the interplay between the orbital and Zeeman interactions of electrons with the magnetic field. The Zeeman interaction produces the

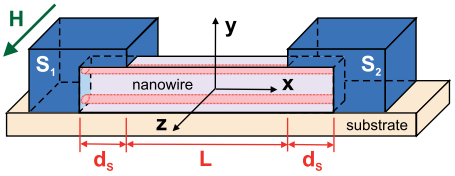

Fig. 13.6: A model Josephson junction with a two-channel nanowire in external magnetic field.

spatial oscillation of the Cooper pair wavefunction at the scale $\hbar v_F/g\mu_B H$ (similar to the ones in SF structures [4]) which result in the magnetic oscillations of the critical current with the period $\hbar v_F/g\mu_B L$, where L is the channel length. If there are several edge states in the system the orbital effect gives rise to the quantum mechanical interference between Cooper pairs propagating along any two different channels. As a result, the critical current oscillates with the periods Φ_0/S_{ij}, where S_{ij} is the area enclosed by the i-th and j-th interfering paths projected on the plane perpendicular to the magnetic field. Finally, the combination of spin–orbit and Zeeman interactions for the special orientations of the magnetic field breaks the inversion symmetry in the direction along the conductive channel. As a result, the usual symmetry relation $I_c(-\varphi) = -I_c(\varphi)$ (φ is the Josephson phase difference) becomes violated and the current–phase relation takes the form $I = I_c \sin(\varphi - \varphi_0)$, where the spontaneous phase φ_0 is determined by the magnetic field.

Below we compare two different approaches based on the Bogoliubov–de Gennes (BdG) and Ginzburg–Landau equations, which are convenient for the description of the Josephson transport through the edge states.

13.3.1 Bogoliubov–de Gennes approach

Let us consider a Josephson system containing only two conductive channels, which model the edge states localized, e.g., at the surface of a single nanowire. The geometry of the system is shown in Figure 13.6. A nanowire (NW) is placed on top of the insulating substrate and put in contact with two superconducting leads S_1 and S_2 with the gap functions $\Delta_s e^{-i\varphi/2}$ and $\Delta_s e^{i\varphi/2}$, respectively. We choose the origin of the Cartesian coordinate system at the middle of the wire. The x-axis is taken along the NW and the y-axis is chosen in the direction perpendicular to the substrate surface. The current–phase relation of the Josephson junction is defined by the dependence of the quasiparticle excitation energies ε on the Josephson phase φ (we put $\hbar = 1$) [47]:

$$I(\varphi) = -2e \sum_{\varepsilon\in(0;\infty)} \frac{\partial\varepsilon}{\partial\varphi} \tanh\left(\frac{\varepsilon}{2T}\right), \tag{13.35}$$

where ε should be found from the BdG equations

$$\begin{pmatrix} \hat{H} & \hat{\Delta} \\ \hat{\Delta}^\dagger & -\hat{H}^\dagger \end{pmatrix} \begin{pmatrix} u \\ v \end{pmatrix} = \varepsilon \begin{pmatrix} u \\ v \end{pmatrix}. \tag{13.36}$$

The electron- and hole-like parts of the quasiparticle wavefunction u and v are multicomponent: $u = (u_{1\uparrow}, u_{2\uparrow}, u_{1\downarrow}, u_{2\downarrow})$ and $v = (v_{1\uparrow}, v_{2\uparrow}, v_{1\downarrow}, v_{2\downarrow})$, where the first indices enumerate the conductive channels and arrows indicate the z-axis spin projections. In Equation (13.36) $\hat{\Delta}$ is the superconducting proximity induced gap and $\hat{H}$ is the single-electron 4×4-matrix Hamiltonian of the isolated wire, which for zero magnetic field takes the form

$$\hat{H} = \left[\xi\left(\hat{p}\right) - \mu + \alpha\hat{p}\hat{\sigma}_z\right] \otimes \hat{I} + \hat{V}(x) \,. \tag{13.37}$$

Here $\hat{p} = -i\partial_x$ is the momentum along the x-axis, $\xi(p)$ is the electron energy in the isolated wire, μ is the chemical potential, the term $\alpha\hat{p}\hat{\sigma}_z$ describes the Rashba spin–orbit coupling due to the broken inversion symmetry in the y-direction [48, 49], $\hat{I}$ is a 2×2 unit matrix in the channel subspace, and the potential $\hat{V}(x)$ describes the scattering at the S/nanowire interfaces. Applying the magnetic field we should include the Zeeman term $g\mu_B H\hat{\sigma}_z$ into (13.37) and replace $\hat{p}$ with $(\hat{p} + |e|A_x/c)$, where $A_x(y) = -Hy$.

Our strategy is to find the quasiclassical solutions of Equation (13.36) inside the nanowire where both $\hat{\Delta}$ and $\hat{V}$ are zero and then to match the solutions at the ends of the wire using phenomenological scattering matrices. As a first step we derive the quasiclassical version of Equation (13.36) inside the wire. Taking, e.g., the functions $u_{1\uparrow}$ and $u_{2\uparrow}$ one can separate the fast oscillating exponential factor: $u_{n\uparrow} = \tilde{u}^{\pm}_{n\uparrow} e^{\pm i p_F^{\pm} x}$, where the Fermi momenta p_F^+ and p_F^- for $p > 0$ and $p < 0$ are different in the presence of the spin–orbit coupling. Then from the BdG equation (13.36) with $\hat{\Delta} = 0$, $\hat{V} = 0$ and $H = 0$ we find:

$$\left[\xi\left(p_F^{\pm}\right) - \mu \pm \alpha p_F^{\pm}\right]\tilde{u}^{\pm}_{n\uparrow} \mp i\left[\xi'\left(p_F^{\pm}\right) \pm \alpha\right]\partial_x \tilde{u}^{\pm}_{n\uparrow} = \varepsilon\tilde{u}^{\pm}_{n\uparrow} \,, \tag{13.38}$$

where $\xi'(p) \equiv \partial\xi/\partial p$. The Fermi momenta are defined by the equations $\xi\left(p_F^{\pm}\right) = \mu \mp \alpha p_F^{\pm}$. Assuming α to be small we find $p_F^{\pm} \approx \left[1 \mp \alpha/\xi'\left(p_F^0\right)\right] p_F^0$ with $\xi\left(p_F^0\right) = \mu$ and obtain:

$$\mp i v_F^{\pm} \partial_x \tilde{u}^{\pm}_{n\uparrow} = \varepsilon\tilde{u}^{\pm}_{n\uparrow} \,. \tag{13.39}$$

The derivation of equations for $u^{\pm}_{n\downarrow}$, $v^{\pm}_{n\uparrow}$ and $v^{\pm}_{n\downarrow}$ is straightforward. Using the expansion $\xi'\left(p_F^{\pm}\right) = \xi'\left(p_F^0\right) \mp \alpha p_F^0 \xi''\left(p_F^0\right)/\xi'\left(p_F^0\right)$, we find the Fermi velocities:

$$v_F^{\pm} = \xi'\left(p_F^0\right) \pm \alpha\left[1 - p_F^0 \xi''\left(p_F^0\right)/\xi'\left(p_F^0\right)\right] \,. \tag{13.40}$$

Clearly the spin–orbit coupling results in the difference between the Fermi velocities v_F^+ and v_F^- of quasiparticles with opposite momenta. This renormalization (13.40) is absent only for exactly quadratic spectrum. It is the difference between v_F^+ and v_F^- which is responsible for the φ_0-junction formation (see [31] and discussion below). Note that another possibility to get the φ_0-junction even for quadratic electron spectrum is to consider nonballistic two-dimensional quasiparticle motion [50, 51].

Introducing the 4-component envelope wavefunctions

$$w^{\pm}_{\sigma}(x) = \left(\sqrt{v_F^{\pm}}\tilde{u}^{\pm}_{1\sigma}, \sqrt{v_F^{\pm}}\tilde{u}^{\pm}_{2\sigma}, \sqrt{v_F^{\mp}}\tilde{v}^{\mp}_{1-\sigma}, \sqrt{v_F^{\mp}}\tilde{v}^{\mp}_{2-\sigma}\right) \tag{13.41}$$

and neglecting the spin flip at the wire ends we can write the matching conditions, e.g., for $w_{\uparrow}^{\pm}$: $w_{\uparrow}^{\pm}(\pm L/2) = \hat{T}^{\pm} w_{\uparrow}^{\pm}(\mp L/2)$, and $w_{\uparrow}^{\mp}(\pm L/2) = \hat{Q}^{\pm} w_{\uparrow}^{\pm}(\pm L/2)$, where L is the wire length, the unitary matrices $\hat{T}^{\pm}$ and $\hat{Q}^{\pm}$ describe the quasiparticle transmission along the wire and both normal and Andreev scattering at the wire ends. The solvability condition $\det\left[\hat{Q}^{-}\hat{T}^{-}\hat{Q}^{+}\hat{T}^{+} - \hat{1}\right] = 0$ [47, 52] for the above matching equations defines the quasiparticle energy spectrum ε. Replacing α and g by $-\alpha$ and $-g$ one finds ε for the opposite spin component.

The general form of the matrices $\hat{T}^{\pm}$ and $\hat{Q}^{\pm}$ is

$$\hat{T}^{\pm} = \begin{pmatrix} e^{ip_{\mathrm{F}}^{\pm}L}\hat{M}^{\pm} & \hat{0} \\ \hat{0} & e^{-ip_{\mathrm{F}}^{\mp}L}\hat{M}^{\mp} \end{pmatrix}, \quad \hat{Q}^{\pm} = \begin{pmatrix} \hat{R}_e^{\pm} & \hat{A}_h^{\mp} \\ \hat{A}_e^{\pm} & \hat{R}_h^{\mp} \end{pmatrix}. \tag{13.42}$$

The 2×2 matrices $\hat{M}^{\pm}$ are defined from the solution of Equation (13.39) under the assumption of different g-factors g_1 and g_2 in different channels:

$$\hat{M}_{nl}^{\pm} = \exp\left[iq^{\pm}L \mp (-1)^n i\pi\phi/2\right]\delta_{nl}, \tag{13.43}$$

where $\phi = HLD/\Phi_0$ is the dimensionless magnetic flux (the channels pass along the plane $y = \pm D/2$), $q^{\pm} = (\varepsilon - g_n\mu_{\mathrm{B}}H)/v_{\mathrm{F}}^{\pm}$ and δ_{nl} is the Kronecker-delta. The phenomenological 2×2 matrices $\hat{R}_{e(h)}^{\pm}$ and $\hat{A}_{e(h)}^{\pm}$ describe the normal and Andreev reflection from the S leads, respectively. The unitarity condition requires these matrices to satisfy the relations $\hat{R}_j^{\pm}\hat{R}_j^{\pm\dagger} + \hat{A}_k^{\mp}\hat{A}_k^{\mp\dagger} = \hat{1}$ and $\hat{R}_j^{\pm}\hat{A}_j^{\pm\dagger} + \hat{A}_k^{\mp}\hat{R}_k^{\mp\dagger} = \hat{0}$, where $j, k \in \{e, h\}$ and $j \neq k$.

For simplicity we restrict ourselves to the case when the quasiparticles experience full Andreev reflection in each channel separately. We assume that such Andreev reflection is caused by the superconducting gap Δ_n induced in the n-th channel due to the proximity effect to the S leads. In the case when the S leads cover the ending parts of the nanowire the asymmetry in the relative position between the channels and the superconductor can result in $\Delta_1 \neq \Delta_2$. The specific values for Δ_n strongly depend on the microscopical properties of S/nanowire interfaces and hereinafter we consider Δ_n to be phenomenological parameters [53–56]. The above assumption of full Andreev reflection means that the size d_s of the induced gap regions (see Figure 13.6) well exceeds the relevant coherence length. In this limiting case the normal scattering vanish ($\hat{R}_e^{\pm} = \hat{R}_h^{\pm} = \hat{0}$) while the Andreev scattering is described by the matrices $(\hat{A}_e^{\pm})_{nl} = \delta_{nl}\exp\left[\mp i\varphi/2 - i\arccos(\varepsilon/\Delta_n)\right]$. Note that for high tunneling rates between the S leads and the conductive channels the quasiparticles reveal Andreev reflection inside the bulk S leads. In our model this situation corresponds to $\Delta_1 = \Delta_2 = \Delta_s$ (Δ_s is the gap in the S leads).

In the short junction limit ($\varepsilon L/v_{\mathrm{F}}^{\pm} \ll 1$) only the subgap Andreev states contribute to the Josephson current. Taking into account all spin projections we obtain four positive subgap energy levels

$$\varepsilon = \Delta_n\left|\cos\left[\varphi/2 - (-1)^n\pi\phi/2 \pm g_n\mu_{\mathrm{B}}HL/v_{\mathrm{F}}^{\pm}\right]\right|, \tag{13.44}$$

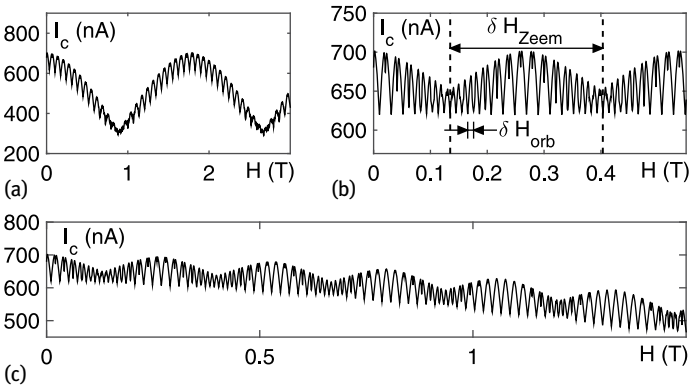

Fig. 13.7: The critical current I_c versus the magnetic field H. We choose $T = 0.1$ K, $\Delta_1 = 7.5$ K, $\Delta_2 = 1$ K, $v_F = 3 \cdot 10^5$ m/s, $L = 2$ μm and (a) $D = 15$ nm and (b)–(c) $D = 50$ nm. We also take (a) $g_1 = g_2 = 1.5$; (b) $g1 = 0$ and $g_2 = 10$; (c) $g1 = 1$ and $g_2 = 10$.

where n enumerates the channels. For large temperatures $T \gg \Delta_n$ the current–phase relation (13.35) takes the form

$$I = \sum_{n=1,2} I_n \sin\left[\varphi + \beta_n H + (-1)^n \pi\phi\right] \cos\left(\gamma_n H\right) \ . \tag{13.45}$$

Here $I_n = |e|\,\Delta_n^2/4\,T$ is the critical current of the n-th channel at $H = 0$, the flux ϕ produces the SQUID-like oscillations of I_c, the cosine term depending on the constants $\gamma_n = g_n \mu_B L \left(1/v_F^+ + 1/v_F^-\right)$ describes the oscillatory behavior of I_c due to the Zeeman interaction similar to the one in SFS structures [4]. The term $\beta_n H = g_n \mu_B L H \left(1/v_F^+ - 1/v_F^-\right)$ describes the φ_0-junction formation due to the spin–orbit coupling [31]. The critical current corresponding to (13.45) reads

$$I_c^2 = I_1^2 \cos^2\left(\gamma_1 H\right) + I_2^2 \cos^2\left(\gamma_2 H\right) + 2 I_1 I_2 \cos\left(\gamma_1 H\right) \cos\left(\gamma_2 H\right) \cos\left[2\pi\phi + \left(\beta_1 - \beta_2\right) H\right] \ . \tag{13.46}$$

Interestingly if $g_1 \neq g_2$ the spin–orbit coupling influences the period of the SQUID-like orbital oscillations in $I_c(H)$, i.e., renormalizes the effective quantization area enclosed by the channels: $S_{\text{eff}} = LD + \Phi_0(\beta_1 - \beta_2)/2\pi$.

Remarkably, the model described in this section allows to reproduce most features of the complicated magnetic oscillation of the critical current experimentally obtained for the Josephson transport through the Bi nanowire. Choosing the parameters relevant to the experimental situation in [46] we obtain a variety of $I_c(H)$ dependencies shown in Figure 13.7. These dependencies reproduce not only multiperiodic oscillations due to the interplay of the orbital and Zeeman interactions observed in [46] but also asymmetry in the form of the upper and lower envelopes. In Figure 13.7a–b one can clearly see two periods of oscillations: $\delta H_{\text{orb}} = \Phi_0/S_{\text{eff}}$ and $\delta H_{\text{Zeem}} = 2\pi/\gamma_1 = 2\pi/\gamma_2$. The slow drift of the average current in Figure 13.7d should be considered in

fact as a fragment of the large-period oscillations caused by the difference between γ_1 and γ_2.

13.3.2 Ginzburg–Landau approach

At temperatures close to T_c it is natural to expect that the system behavior can be described by the Ginzburg–Landau model modified to include the Zeeman and spin–orbit interactions. First, we consider the simplest case when there is only one conductive channel of the length L connecting the superconducting leads of the Josephson junction. We again assume that the magnetic field $\boldsymbol{H} = H\hat{\boldsymbol{z}}$ is perpendicular to the channel and the sample edge breaks the inversion symmetry in the y-direction which results in strong spin–orbit coupling of the Rashba type. Then at temperatures close to the superconducting transition temperature T_c the expansion of the free energy F up to the terms $\sim O(\Psi^2)$ has the form [57, 58]

$$F = \int \left\{ a\,|\Psi|^2 + \gamma \left|\hat{D}_x \Psi\right|^2 + \beta \left|\hat{D}_x^2 \Psi\right|^2 - \nu H \left[\Psi \left(\hat{D}_x \Psi\right)^* + \Psi^* \left(\hat{D}_x \Psi\right)\right]\right\} dx\,, \qquad (13.47)$$

where Ψ is the superconducting order parameter in the conductive channel, $a(x) \sim [T - T_c(x)]$ and inside the channel $a > 0$, $\hat{D}_x = -i\partial_x + 2\pi A_x/\Phi_0$ ($A_x = -Hy$ is the vector potential) and the constant $\nu \sim g\alpha$ describes the strength of the spin–orbit coupling. In (13.47) the constant γ is determined by the Zeeman interaction and as a result the profile $\Psi(x)$ inside the channel strongly depends on the ratio between H and the field H_L corresponding to the tricritical Lifshitz point. For $H < H_L$ one has $\gamma > 0$ and Ψ monotonically decays from the superconducting leads towards the center of the channel. In contrast, when $H > H_L$ (above the Lifshitz point) γ becomes negative giving rise to the damped oscillatory behavior of the Cooper pair wavefunction due to the formation of the FFLO state [4]. In the latter case one should take into account the higher order gradient term with $\beta > 0$ in (13.47) which provides an additional length-scale $\xi_f = 2\sqrt{\beta/|\gamma|}$ characterizing the period of the gap function oscillation.

To calculate the Josephson current–phase relation we assume that: (i) the spin–orbit coupling is weak and can be treated perturbatively; (ii) $L \gg \sqrt{\xi^2 + \xi_f \xi}$ where $\xi = \sqrt{|\gamma|/a}$; (iii) inside the S leads the Zeeman interaction is negligible; (iv) the conductivity of the S leads well exceeds the one in the wire so the inverse proximity effect can be neglected; (v) the interfaces between the channel and the superconducting leads are absolutely transparent for electrons. The latter assumption results in the continuity of the order parameter at the interfaces $x = \pm L/2$ so that $\Psi(\pm L/2) = \Delta \exp(\pm i\varphi/2)$, where Δ and φ are the absolute value and phase of the gap function in the superconductors.

Varying the free energy $\int F dx$ with respect to Ψ^* and A_x and excluding the effect of the vector potential (which is constant along the wire) by introducing the new function

$\psi(x) = \Psi(x)\exp\{-2\pi i A_x x/\Phi_0\}$ we obtain the equations

$$a\psi - \partial_x(\gamma\partial_x\psi) + \partial_x^2\left(\beta\partial_x^2\psi\right) + iH\left[\partial_x(\nu\psi) + \nu\partial_x\psi\right] = 0 \tag{13.48}$$

and the expression for the superconducting current

$$j = \frac{4c}{\Phi_0}\left\{\Im\left[\gamma\psi^*\partial_x\psi + \beta\left(\partial_x^2\psi\partial_x\psi^* - \psi^*\partial_x^3\psi\right)\right] - \nu H|\psi|^2\right\}, \tag{13.49}$$

where $\Phi_0 = \pi\hbar c/|e|$ is the superconducting flux quantum.

Equations (13.48) should be supplemented by four boundary conditions. The first two conditions reflects the continuity of the order parameter at the ends of the channel $x = \pm L/2$: $\psi(\pm L/2) = \Delta\exp(\pm i\tilde{\varphi}/2)$, where $\tilde{\varphi} = \varphi/2 + 2\pi A_x L/\Phi_0$ is the gauge-invariant phase difference between the superconductors. The second pair of conditions can be obtained by the integration of Equation (13.48) over a small region near the interfaces. Neglecting the Zeeman interaction inside the superconductors and the inverse proximity effect one obtains that $-\gamma\partial_x\psi + \beta\partial_x^3\psi + i\nu H\psi\big|_{x=\pm L/2} = 0$.

The solution of Equation (13.48) strongly depends on the system parameters. The simplest situation is realized when the magnetic field is well below the tricritical point so that the coefficient γ is positive and not small. In this case the term $\propto \beta$ in the free energy (13.47) is small and can be neglected. Then the solution of Equation (13.48) takes the form $\psi(x) = A_+\exp(q_+x) + A_-\exp(q_-x)$, where $q_\pm = \frac{i\nu H}{\gamma} \pm \sqrt{\frac{a}{\gamma} - \frac{\nu^2H^2}{\gamma^2}}$ are the roots of the characteristic equation $a - \gamma q^2 + 2i\nu Hq = 0$. Note that the absence of the intrinsic superconductivity in the channels requires $a > a_c = \nu^2H^2/\gamma$. Taking into account the continuity of the order parameter at $x = \pm L/2$ one finds the constants $A_\pm$ and, thus, the superconducting current (13.49). To make the results more transparent we will focus only on the long junction limit ($L\sqrt{(a-a_c)/\gamma} \gg 1$). In this case each exponent in the function $\psi(x)$ is localized near the corresponding superconducting lead and can be considered independently from another one. From the boundary conditions we find $A_\pm = \Delta\exp(\pm i\tilde{\varphi}/2 \mp q_\pm L/2)$ and substitute the resulting profile $\psi(x)$ into Equation (13.49). Assuming the spin–orbit coupling to be small we treat only correction $\propto \nu$ in the wavevectors q and neglect the effect of the spin–orbit coupling in the exponential prefactors. Then the current–phase relation takes the form

$$j(\tilde{\varphi}) = j_c\sin(\tilde{\varphi} - \varphi_0), \tag{13.50}$$

where $j_c = (4c/\Phi_0)\gamma\Delta^2\sqrt{(a-a_c)/\gamma}\exp\left(-\sqrt{(a-a_c)\gamma}L\right)$ is the critical current and $\varphi_0 = \nu HL/\gamma$.

The current–phase relation (13.50) implies that the minimum of the junction energy $E \propto -j_c\cos(\tilde{\varphi} - \varphi_0)$ corresponds to the nonzero phase difference $\tilde{\varphi} = \varphi_0$, which is determined by the spin–orbit coupling and the magnetic field. In contrast with the π-junctions where the transitions between 0 and π states occur as a phase jump accompanied by the vanishing of the critical current, here φ_0 as a function of H is changing continuously and the critical current remains nonzero.

Now we turn to the more interesting situation when the magnetic field is close to the tricritical point and in (13.47) the coefficient γ is small (the solution of the Ginzburg–Landau equation exactly at the tricritical point is considered in [59]). In this case the solution of Equation (13.48) inside the channel is the sum of 4 exponents of the form $\exp(qx)$ with q satisfying the equation $a - \gamma q^2 + \beta q^4 + 2i\nu Hq = 0$. If the spin–orbit coupling constant $\nu \ll 1$ this equation can be solved perturbatively. Taking $q = q_0 + q_1$, where $q_n \propto \nu^n$, in the zeroth order we get $q_0^2 = \frac{2\ \mathrm{sign}(\gamma)}{\xi_f^2}(1 + i\mu\sqrt{\xi_f^2/\xi^2 - 1})$, where $\xi = \sqrt{|\gamma|/a}$ and $\mu = \pm 1$. One sees that if the magnetic field is well below the tricritical point so that $\xi > \xi_f$ the wavevector q_0 is real. This situation is qualitatively equivalent to the case described above. However when $\xi < \xi_f$ the imaginary component of q_0 appears and the order parameter reveals spatial oscillations. These oscillations result in a series of transitions between the 0- and π-states which are revealed through vanishing of the critical current. Note that for $\gamma < 0$ the absence of the intrinsic superconductivity in the channel requires $\xi < \xi_f$ (otherwise $\psi(x)$ would be an oscillating function whose amplitude does not depend on the distance from the superconducting lead).

Let us analyze the case $\xi < \xi_f$ for arbitrary sign of γ. Introducing the values $k^{\pm} = \xi_f^{-1}\sqrt{\xi_f/\xi \pm 1}$ we obtain the following solutions for q_0:

$$q_0 = \begin{cases} \lambda\,(k^- - i\mu k^+) & \text{for } \gamma < 0, \\ \lambda\,(k^+ + i\mu k^-) & \text{for } \gamma > 0, \end{cases} \tag{13.51}$$

where $\lambda = \pm 1$. Then in the first order of the perturbation theory we find $q_1 = \mu s$, where $s = -\nu H\,\mathrm{sign}(\gamma)/\,(4\beta k^+ k^-)$.

Let us first treat the case $\gamma < 0$ in detail (for $\gamma > 0$ one has to replace $k^- \to k^+$ and $k^+ \to -k^-$ in the final answers). For simplicity we assume the junction to be long so that $k^- L \gg 1$. In this case one may consider the superconducting nuclei with $\lambda = -1$ (localized near the left end of the channel) and the ones with $\lambda = +1$ (localized near the right end) independently. Taking into account the boundary conditions at $x = \pm L/2$ and neglecting the effect of the spin–orbit coupling in the exponential prefactors we find:

$$\psi(x) = \frac{\Delta}{2}\sum_{\lambda,\mu=\pm 1}\left(1 + i\mu\frac{k^-}{k^+}\right)e^{i\lambda\bar{\varphi}/2 + [\lambda(k^- - i\mu k^+) + \mu s](x - \lambda L/2)}\,. \tag{13.52}$$

Substituting (13.52) into (13.49) and accounting for the effect of the spin–orbit coupling only inside the arguments of exponents we again obtain the current–phase relation of the form (13.50), where $\sin\varphi_0 = \cosh(sL)\sin\chi/\sqrt{\sin^2\chi + \sinh^2(sL)}$,

$$j_c = \frac{32\sqrt{2}c\beta\Delta^2 k^-}{(\xi_f\xi)^{3/2}\Phi_0 k^+}e^{-k^- L}\sqrt{\sin^2\chi + \sinh^2(sL)}\,, \tag{13.53}$$

and $\cos(\chi - k^+ L) = k^+\,(\xi_f - 2\xi)\,\sqrt{\xi/(2\xi_f)}$.

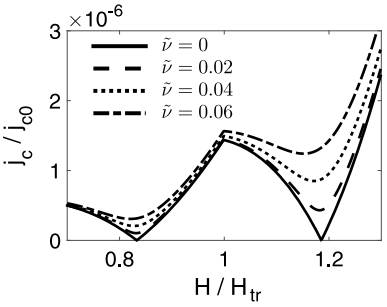

Fig. 13.8: The dependencies of the critical current j_c as a function of the applied magnetic field H. The critical current is scaled by the value $j_{c0} = 32\sqrt{2}c\gamma_0^{3/2}\Delta^2/\Phi_0\sqrt{\beta}$. Different curves correspond to different values of the parameter $\tilde{\nu} = \nu H_{tr}/4\gamma_0$ describing the strength of the spin–orbit coupling. We take $2\sqrt{\beta/\gamma_0} = 1$ and $\sqrt{\gamma_0/a} = 0.5$.

Interestingly, the spin–orbit coupling not only causes the φ_0-junction formation but also affects the critical current. Indeed, for long junctions with $L \sim s^{-1}$ the term $\sinh^2(sL)$ can result in the increase in I_c with the increasing H. Obviously this effect can be suppressed because of damping of the superconductivity inside the S leads due to the magnetic field. However for the Pb films and $LaAlO_3/SrTiO_3$ heterostructures with strong spin–orbit coupling in rather small magnetic fields the increasing dependencies $T_c(H)$ were observed [60]. In this case as follows from (13.53) the dependencies $I_c(H)$ should reveal the increasing trend due to the spin–orbit coupling. Note also that the Zeeman interaction causes the sign change of the coefficient γ near the tricritical point, which results in the nonmonotonic dependencies of the critical current as a function of H. Expanding $\gamma = \gamma_0\,(1 - H/H_{tr})$ (here H_{tr} is the field corresponding to the Lifshitz point) one obtains the dependencies $j_c(H)$ shown in Figure 13.8. One sees that if there is no spin–orbit coupling the critical current turns to zero at the points of the transition between 0- and π-states while in the presence of the spin–orbit coupling I_c stays finite. Note also that if there are several conductive channels the dependencies $I_c(H)$ reveal the usual Fraunhofer oscillation which was described in detail in Section 13.3.1. The origin of these oscillations is the difference in the vector potential entering the gauge invariant phase $\tilde{\varphi}$ for different channels.

13.4 Mesoscopic fluctuations

The existing experiments [23–25, 61] demonstrating the anomalously slow decay of superconducting correlations in ferromagnets in the absence of a noncollinear magnetization and with the questionable strength of the spin–orbit effects force theoreticians to look for other possible sources of the suppression of the interference of random quasiparticle trajectories. Motivated by the above discrepancy between the experiment and theory we reexamine the standard Usadel-type model and search for its possible shortcomings which can reveal themselves in the estimates of the length of decay of superconducting correlations in a dirty ferromagnet. One of the most important assumptions which form the basis of the Usadel theory is that we operate with

the ensemble-averaged Green functions neglecting, thus, possible fluctuations of the measurable quantities due to the random distribution of impurities [62–64]. In the case of the dirty ferromagnet this assumption is crucial to obtain the exponential decay of the anomalous Green function at the length ξ_f. Indeed, the motion of quasiparticles in a ferromagnetic metal occurs along the random quasiclassical trajectories which experience sharp turns at the impurity positions. As it has been noted in the introduction, the exchange field is responsible for the relative phase γ gained between the electronic and hole parts of the quasiparticle wavefunction along these trajectories. Averaging the Green functions we average in fact the exponential phase factor $e^{i\gamma}$ with the random phase γ depending on the trajectory length obtaining naturally an exponentially decaying quantity $\propto e^{-x/\xi_f}$, where x is the distance from the SF interface. This destructive interference cannot play such a dramatic role when we calculate root-mean-square (rms) values due to a partial phase gain compensation in squared quantities. Considering, e.g., the supercurrent I of the SFS Josephson junction we can introduce the rms value of the current as follows: $\delta I = \sqrt{\langle I^2\rangle - \langle I\rangle^2}$. The compensation of the phase factor γ can occur only for correlated random trajectories passing at the distance not exceeding the Fermi wavelength $\lambda_F = 2\pi/k_F$. This restriction causes the reduction of the δI value by a factor of $\sqrt{N}$, where N is the number of transport channels in the junction. Finally, we obtain $\delta I/\langle I\rangle \sim e^{d/\xi_f}/\sqrt{N}$, where d is the distance between the S electrodes [65]. The number of channels can be of course pretty large: $N \sim k_F L$ for two dimensional and $N \sim (k_F L)^2$ for three dimensional junctions with the transverse dimension L. Nevertheless the current fluctuations can strongly exceed the average value at large distances d well above the coherence length ξ_f. In this sense these fluctuations are giant compared to the ones in superconductor–normal metal–superconductor (SNS) junctions where the value $\delta I \sim e\Delta_0/\hbar$ for short junctions with $d \ll \xi_s$ [47] is known to be determined by the universal conductance fluctuations [66, 67] or even smaller for long junctions with $d \gg \xi_s$ [68]. Here Δ_0 is the gap in the bulk superconductor and ξ_s is the superconducting coherence length. Experimentally, in each particular sample we can expect to measure a random critical current value which should exhibit giant sample-to-sample fluctuations. Thus, in a given experiment one can easily obtain the critical current well above the limit imposed by the Usadel theory which can give us only the average current value. The above arguments and standard Landauer relation between the normal junction resistance R and the N number make it possible to guess a simple estimate for the fluctuating critical current:

$$\delta I \sim \Delta_0/\sqrt{\hbar R}\,. \tag{13.54}$$

Note that this inverse square root dependence differs strongly from the standard relation $I_c \sim \Delta_0/(eR)$ for the SNS junction. Our further calculations nicely confirm the above δI estimate and, thus, the observation of this unusual relation between the supercurrent and normal junction resistance could provide a verification of the long range proximity mechanism caused by mesoscopic fluctuations. The ensemble aver-

aging laying in the basis of the derivation of the Usadel equations from the quasiclassical Eilenberger theory overlooks the above fluctuation effects emerging at mesoscopic scales. These fluctuation effects reveal themselves even in the quasiclassical limit $\lambda_F \to 0$ when we can neglect the corrections found in [63, 64] which vanish in this limit corresponding to a large junction conductance.

We proceed with a detailed consideration of the critical current fluctuations in the SFS junction and for this purpose we use an approach based on the averaging over the random quasiparticle trajectories passing in the field of point scatterers (see [69] for review). For each random trajectory inside the F layer one can consider the 1D problem for propagating electrons and holes experiencing Andreev reflection at the point where the trajectory touches the left or right S electrode. We start from the case $d \ll \xi_s$ and assume the superconducting gap (exchange field) to vanish inside (outside) the F layer. Thus, we neglect the so-called inverse proximity effect, i.e., the mutual influence of the order parameters at the interface. The current–phase relation for the short junction limit can be defined only from the spectra of the subgap Andreev states at the trajectories ending at both the left and right S electrodes $\epsilon = \pm\Delta_0 \cos\left((\varphi \pm \gamma)/2\right)$ neglecting the contributions from the states above the gap. Here φ is the phase difference between the S electrodes, and $\pm\gamma$ is the spin-dependent phase shift between the electron- and hole-like parts of the total wavefunction along the quasiclassical trajectory Γ_{12}. Each trajectory Γ can touch each of the S electrodes only once otherwise part of the trajectory Γ touching the same electrode two times can be considered separately and the corresponding spectrum does not depend on the phase difference φ. Certainly, there exist trajectories of the length exceeding ξ_s with the quasiparticle spectrum consisting of several subgap branches but the probability to get such trajectories vanishes for short junctions. According to the procedure suggested in [20] the phase shift γ can be determined from Equations (13.13) and (13.14) which formally coincide with the Eilenberger-type equations written for the singlet and triplet parts of the anomalous quasiclassical Green function $f = f_{\text{sing}} + \boldsymbol{f}_t\hat{\sigma}$ and zero Matsubara frequencies.

The boundary conditions at the left electrode read: $f_{\text{sing}}(s = s_L) = 1, \boldsymbol{f}_t(s = s_L) = 0$. The function $f_{\text{sing}}(s = s_R) = \cos\gamma$ taken at the right S electrode determines the phase gain γ along the trajectory. Let us emphasize here that contrary to the standard consideration the Eilenberger-like equations in our approach are written along a random trajectory with many sharp turns and therefore they do not contain the impurity terms.

Summing up over all trajectories Γ we find the current–phase relation:

$$I = \sum_{\Gamma} \left(j(\varphi + \gamma) + j(\varphi - \gamma)\right)(\boldsymbol{n}_F, \boldsymbol{n}_L)\,, \tag{13.55}$$

where $j(\chi)$ is defined by Equation (13.4). The vectors $\boldsymbol{n}_L$ and $\boldsymbol{n}_F$ are the unit vectors normal to the left electrode surface and parallel to the trajectory direction, respectively. The vector $\boldsymbol{n}_F$ parametrizes random quasiparticle trajectories outcoming from the left electrode. The random phase γ depends on the whole path between the elec-

trodes and not just on the distance between the starting and ending points of the trajectory. Taking for simplicity the case of a homogeneous exchange field we find $\gamma = 2\,\mathrm{h}(s_R - s_L)/\hbar v_\mathrm{F} = \Omega t$, where t is the time of flight of electron along the trajectory and $\Omega = 2\,\mathrm{h}/\hbar$.

Our next step is the averaging of the above Josephson current expression over the random time of flight t. For this purpose we need to introduce the distribution function describing the probability density $w(\boldsymbol{r}_2, \boldsymbol{r}_1, t)$ to get the trajectory starting at a certain point $\boldsymbol{r}_1$ at the left electrode at the time $t_1 = 0$ and touching the right electrode at an arbitrary point $\boldsymbol{r}_2$ at the time $t_2 = t$. In the diffusion limit this probability density is almost independent on the quasiparticle velocity direction at the electrodes and satisfies the diffusion equation:

$$\frac{\partial}{\partial t} w = D \frac{\partial^2}{\partial \boldsymbol{r}_2^2} w + \delta(\boldsymbol{r}_2 - \boldsymbol{r}_1)\delta(t)\ . \tag{13.56}$$

Here we assume the elastic mean free path ℓ to be less than all the relevant length scales so that, in particular, one takes $\ell \ll \xi_f$. The boundary condition should be defined from the fact that the trajectory which touches the S electrodes do not contribute to the total probability density any more. An obvious reason is that the corresponding electron moving along the trajectory experiences in this case the full Andreev reflection. Thus, at the surfaces of both S electrodes we should put $w = 0$. Choosing $\boldsymbol{r}_{1,2}$ at the left and right electrodes, respectively, we find the probability distribution $P(t)$ for the first-passage time between two electrodes:

$$P(t) = -\int\limits_{S_R} D\left(\boldsymbol{n}_R \frac{\partial}{\partial \boldsymbol{r}_R}\right) w(\boldsymbol{r}_R, \boldsymbol{r}_L, t) ds_R\ , \tag{13.57}$$

where the integral is taken over the surface of the right electrode and $\boldsymbol{n}_R$ is the unit vector normal to this surface. The value $P(t)$ gives the probability of the trajectory starting at the point $\boldsymbol{r}_L$ at $t_1 = 0$ to leave the junction in the time interval from t to $t + dt$. The average current can be written as follows:

$$\langle I \rangle = \sum_{n\geq 1} N j_n \sin n\varphi \langle \cos n\gamma \rangle\ , \tag{13.58}$$

where $\langle \cos n\gamma \rangle = Re \int_0^\infty e^{-in\Omega t} P(t) dt = ReP(n\Omega)$. We assume here the surfaces of S electrodes to be flat and obtain a one-dimensional problem along the coordinate x perpendicular to these surfaces. Introducing the function $W(x, t)$ satisfying the 1D diffusion equation $DW''_{xx} - in\Omega W = 0$ with the boundary conditions $DW(x = 0) = \ell$ and $W(x = d) = 0$ one can find $P(n\Omega) = DW'_x(x = d, n\Omega)$.

Substituting the solution of the above diffusion equation into the current we obtain:

$$\langle I \rangle = Re \sum_{n\geq 1} N j_n \sin n\varphi \frac{\ell\sqrt{in}}{\xi_f} \frac{1}{\sinh\left[\sqrt{in}\, d/\xi_f\right]}\ . \tag{13.59}$$

One can see that this expression reproduces the result of the Usadel theory only for the first harmonic $I_1 \propto \sin\varphi$ in the current–phase relation [35]. The length L_n of the exponential decay of higher harmonics $I_n \propto \sin n\varphi$ appears to exceed the appropriate length in the Usadel-type calculation: we obtain here $L_n = \xi_f/\sqrt{n}$ instead of $L_n = \xi_f/n$. This result indicates an obvious increase of the range of superconducting correlations due to mesoscopic fluctuations and originates from the incorrect calculation of the ensemble averages of the product of the anomalous Green functions in the ferromagnet within the Usadel theory. This failure of the Usadel-type consideration is caused by the appearance of the random interference phase γ and occurs only in the nonlinear regime of rather strong superconducting correlations. Indeed, considering, e.g., the value $\langle\cos 2\gamma\rangle$ in the above derivation we calculate the average $\langle|f_{\rm sing}|^2 - |f_t|^2\rangle$ which definitely differs from the product of averages $\langle f_{\rm sing}\rangle\langle f^*_{\rm sing}\rangle - \langle f_t\rangle\langle f^*_t\rangle$. Note that the above approach describes the fluctuation contributions which do not vanish in the limit $\lambda_{\rm F} \to 0$ and can, thus, exceed the corrections found previously in [64]. Our contributions are caused by the quantum interference effects associated with a much larger wavelength $\hbar v_{\rm F}/h$ of the quasiparticle wavefunction envelope.

To find the rms value of the supercurrent we evaluate now the expression

$$\langle I^2\rangle = \sum_{I,\tilde{I},n,m} j_n j_m A_{nm}(\boldsymbol{n}_F, \boldsymbol{n}_L)(\tilde{\boldsymbol{n}}_F, \tilde{\boldsymbol{n}}_L)\sin n\varphi \sin m\varphi\,, \tag{13.60}$$

where $A_{nm} = \langle\cos n\Omega t \cos m\Omega\tilde{t}\rangle$. The calculation of the above double sum can be done similar to the calculation of the conductance $R^{-1} = G(d, \ell)$ in a dirty wire above $T_{\rm c}$. Assuming the normal layer thickness to be rather large ($d \gg \xi_f$) and omitting the averages of the fast oscillating phase factors (which should give the short-range terms decaying at the length ξ_f) we get

$$\langle I^2\rangle \simeq (G(\tilde{d}, \tilde{\ell})/4G_0)\sum_{n\geq 1} j_n^2 \sin^2 n\varphi\,, \tag{13.61}$$

where $G_0 = e^2/\pi\hbar$, $\tilde{d} = \Omega d/k_{\rm F}v_{\rm F}$ and $\tilde{\ell} = \Omega\ell/k_{\rm F}v_{\rm F}$. Taking the Drude-type conductance $G/G_0 = N\ell/d$ for a disordered wire of the length d we find the estimate

$$\sqrt{\langle I^2\rangle - \langle I\rangle^2} \sim \sqrt{\frac{N\ell}{d}}\sqrt{\sum_{n\geq 1} j_n^2 \sin^2 n\varphi}\,. \tag{13.62}$$

The deviations from the Drude result arise naturally from the so-called interference or localization corrections to the conductance [69]. Perturbatively, they can be estimated as terms arising from the paths with self-crossings in the above double sum over the trajectories. According to the Thouless criterion [70] the localization effects in a disordered wire are small provided the effective number $N\ell/d$ of the conducting modes is large. Thus, one can expect our Drude-type estimate to hold in the case $N\ell/d \gg 1$. In the opposite limit the wire conductance in Equation (13.61) and, thus, the rms value of the critical current decay exponentially at the length $N\ell$.

Comparing the rms value with the average current taken in the same limit $d \gg \xi_f$ we find

$$\delta I/\langle I\rangle \sim \sqrt{\frac{\xi_f^2}{N\ell d}}\exp\left(\frac{d}{\xi_f\sqrt{2}}\right). \tag{13.63}$$

This expression for current fluctuations definitely cannot be obtained within the averaged Usadel theory and results from the partial cancelation of the interference contributions in the product of the anomalous Green functions. Note that turning to the limit $d \ll \xi_f$, i.e., to the case of the SNS junction our consideration should give a vanishing δI value since we disregarded the quantum interference of random semiclassical trajectories responsible for standard mesoscopic fluctuations [47]. The effect of these fluctuations on the critical current through the SNS junction is similar to the phenomenon of universal conductance fluctuations and gives the value $\delta I \sim e\Delta/\hbar$ proportional to the single-mode contribution to the supercurrent. Despite the small factor $N^{-1/2}$ in Equation (13.63) the current fluctuations for $d \gg \xi_f$ appear to be giant compared to the current average value which decays exponentially at the small distance ξ_f. The rms value can well exceed the Josephson current quantum $e\Delta/\hbar$ in SNS junctions [47]. It is also important to note that contrary to the average current the fluctuating contributions to higher harmonics of the current–phase relation are not suppressed exponentially compared to the first harmonic. This strong anharmonicity probably relates to the experimental data on the large second harmonics in SFS junctions [13, 71]. Certainly, in realistic junctions the above assumption of the full Andreev reflection at the SF boundaries can be broken due to the effect of the interface potential barriers which certainly suppress the higher current harmonics. Still the main effect, namely, the partial compensation of the phases γ in the rms values should exist even in the presence of the barriers though, of course, the above procedure of averaging over the random trajectories should be modified.

The rms value decays with the increase of the distance between the S electrodes, however, this decay follows only the inverse square root law instead of the exponential decay of the average current. Taking the distance d larger than ξ_s we can no longer use, of course, the short junction approximation. However, one can easily see that the above long-range behavior of the critical current fluctuations holds even in this regime at least for the first harmonic in the current–phase relation. Indeed, the critical current in this limit is determined by the singlet component of the anomalous Green function $\sum_\Gamma f_{sing\Gamma} = \sum_\Gamma \cos\gamma_\Gamma$. The average current, therefore, decays exponentially as $\langle I\rangle \propto (\ell N/\xi_f)e^{-d/\xi_f\sqrt{2}}$ while the rms average becomes long-range because of the partial phase compensation at close trajectories: $\langle(\delta I)^2\rangle \propto \langle f_{\rm sing}^2\rangle \propto N\ell/d$. Thus, the above calculations confirm the estimate (13.54) both for short and long junctions. Certainly, further increase in the distance d will give us the exponential decay of the supercurrent but at the distances exceeding the normal metal coherence length $\sqrt{D/T}$. It is interesting to note that taking, e.g., the gap $\Delta_0 \sim T_c \sim 3$–4 K and the resistance $R \sim 10$–$100\ \Omega$ from the experiment [25] on Co nanowires with W electrodes and using

the Equation (13.54) we get the value $\delta I \sim 1\,\mu A$, which is only an order of magnitude less that the critical current observed in [25]. The remaining discrepancy is probably caused by the overestimating of the wire resistance in Equation (13.54) due to the presence of contact resistances in the system.

Finally, we briefly comment on the effect of mesoscopic fluctuation on the local density of states (LDOS) at the Fermi level. In the ballistic system for straight linear trajectories one can easily obtain an appropriate Eilenberger-type expression for this quantity as a sum of contributions from different quasiclassical paths. This expression can be simplified applying the normalization condition for quasiclassical Green functions and taking the perturbation expansion in powers of the f function (see, e.g., [72] for convenient notations). Generalizing this expressions for the trajectories experiencing many sharp turns one can get: $\delta\nu/\nu_F \propto -N^{-1}\sum_\Gamma(|f_{sing}|^2 - |f_t|^2)$, where ν_F is the normal metal LDOS. The ensemble average of this value certainly decays exponentially $\langle\delta\nu/\nu_F\rangle \propto -\langle\cos 2\gamma\rangle \propto -(\ell/\xi_f)e^{-d/\xi_f}\cos(d/\xi_f + \pi/4)$ with the increase in the distance d from the S electrode. The fluctuating LDOS contains a long-range contribution similar to the one calculated above for the critical current: $\sqrt{\langle(\delta\nu/\nu_F)^2\rangle} \propto \sqrt{\ell/dN}$. This nonexponential behavior of the fluctuating superconducting contribution to the LDOS could be measured by a local conductance probe at different points of a ferromagnetic nanowire placed in contact with a superconductor providing, thus, a possible explanation of the long-range proximity effect observed in [23, 24, 61, 73, 74].

The direct observation of the giant sample-to-sample fluctuations assumes the measurements of the critical current or LDOS on different junctions. It would be much more convenient to find the way to change the interference phases γ i n a given sample and measure the junction "fingerprints" in analogy to the observation of universal conductance fluctuations vs applied magnetic field [75]. Indeed, such type of experiment in the SFS junctions may become possible provided we apply the magnetic field which can affect the domain structure in the ferromagnetic layer without producing noncollinear magnetic regions to avoid the admixture of the long-range triplet correlations. Note finally, that the mesoscopic fluctuations considered in our work should be most easily observed in the experiments with the ferromagnetic wires because their relative contribution decays with the increase of the number of transport modes in the junction.

13.5 Conclusion

To sum up, in this chapter we have shown that the spin splitting of the electronic Fermi surfaces due to the exchange field and/or the spin–orbit coupling gives rise to very rich interference physics. The most dramatic consequences of such interference appear in Josephson junctions with a ferromagnetic weak link. When propagating inside the ferromagnetic material the electrons gain a phase which is determined mainly by the interplay between the two length scales: the period of the FFLO oscillations and

the length of the electron trajectory. The constructive interference among the certain trajectories significantly enhance the proximity effect and modifies the current–phase relation of the SFS/ Josephson junctions. Moreover, the spin-dependent renormalization of the electron Fermi velocity due to the spin–orbit coupling results in the appearance of the spontaneous ground state Josephson phase φ_0 which can be effectively controlled by the magnetic or exchange field. Surprisingly, even in the presence of strong disorder the quantum interference affects the properties of the Josephson systems due to the mesoscopic fluctuations. The resulting renormalization of the Josephson current–phase relation can explain the experimental data showing the anomalously slow decay of superconducting correlations in ferromagnets.

Note that in all sections of this chapter we discuss mainly the effects caused by the superconducting correlations with zero spin projection S_z on the exchange field direction. However if the ferromagnet contains several domains with the noncollinear magnetic moments the triplet correlations with $S_z = \pm 1$ appear. Such correlations are not sensitive to the exchange field and penetrate the ferromagnets over the long distances giving rise to the so-called long-range triplet proximity effect [5]. The presence of the long-range triplet correlations gives rise to a series of unusual phenomena controlled by the quantum interference such as triplet spin–valve effect in $S/F_1/F_2$ and $F_1/S/F_2$ systems [76, 77] and the long-range Josephson effect in $S/F_1/F/F_2/S$ junctions [30]. Also the effect of the triplet correlations on the electron interference plays the crucial role in the fast growing field of the superconducting spintronics which involves the spin degree of freedom into the functionality of electronic devices [7].

Thus, the interference phenomena described in this chapter show the richness of the proximity effect physics in superconductor/ferromagnet hybrids and provide design guidelines for the next generation of tunable elements found in cryogenic computational electronics.

Acknowledgment: We thank A. V. Samokhvalov, R. Shekhter, H. Bouchiat, and S. Guéron for useful discussions. This work was supported by the French ANR "MASH" and "SUPERTRONICS," NanoSC COST Action MP1201, Russian Science Foundation under Grant No. 15-12-10020 (ASM, Section 13.4), and Russian Foundation for Basic Research under Grants No. 15-42-02195 (ASM, Section 13.2) and No. 16-02-00815A (SVM, Section 13.3).

Bibliography

[1] Ginzburg VL. "Ferromagnetic superconductors," Zh. Eksp. Teor. Fiz. 31:202, 1956 [Sov. Phys. JETP 4:153, 1957].
[2] Saint-James D, Sarma D, Thomas EJ. 1969, Type II Superconductivity (Pergamon, New York).
[3] Aoki D, Flouquet J. J. Phys. Soc. Japan 83:061011, 2014.
[4] Buzdin AI. Rev. Mod. Phys. 77:935, 2005.

[5] Bergeret FS, Volkov AF, Efetov KB. Rev. Mod. Phys. 77:1321, 2005.
[6] Eschrig M. Rep. Prog. Phys. 78:104501, 2015.
[7] Linder J, Robinson JWA. Nat. Phys. 11:307, 2015.
[8] Golubov A, Kupriyanov M, Ilichev E. Rev. Mod. Phys. 76:411, 2004.
[9] Fulde P, Ferrell RA. Phys. Rev. 135:A550, 1964.
[10] Larkin AI, Ovchinnikov YN. Zh. Eksp. Teor. Fiz. 47:1136, 1964 [Sov. Phys. JETP 20:762, 1965].
[11] Buzdin AI, Bulaevskii LN, Panyukov SV. Pis'ma Zh. Eksp. Teor. Fiz. 35:147, 1982 [JETP Lett. 35:178, 1982].
[12] Ryazanov VV, Oboznov VA, Rusanov AYu, Veretennikov AV, Golubov AA, Aarts J. Phys. Rev. Lett. 86:2427, 2001.
[13] Oboznov VA, Bol'ginov VV, Feofanov AK, Ryazanov VV, Buzdin AI. Phys. Rev. Lett. 96:197003, 2006.
[14] Blanter YaM, Hekking FWJ. Phys. Rev. B 69:024525, 2004.
[15] Buzdin AI, Melnikov AS, Pugach NG. Phys. Rev. B 83:144515, 2011.
[16] Radovic Z, Ledvij M, Dobrosaljevic-Grujic L, Buzdin AI, Clem JR. Phys. Rev. B 44:759, 1991.
[17] Kehrle J, Zdravkov VI, Obermeier G, Garcia-Garcia J, Ullrich A, Müller C, Morari R, Sidorenko AS, Horn S, Tagirov LR, Tidecks R. Annalen der Physik 524:37, 2012.
[18] Robinson JWA, Witt JDS, Blamire MG. Science 329:59, 2010.
[19] Khaire TS, Khasawneh MA, Pratt WP Jr, Birge NO. Phys. Rev. Lett. 104:137002, 2010.
[20] Melnikov AS, Samokhvalov AV, Kuznetsova SM, Buzdin AI. Phys. Rev. Lett. 109:237006, 2012.
[21] Samokhvalov AV, Shekhter RI, Buzdin AI. Scientific Reports 4:5671, 2014; J. Phys. Conf. Ser. 568:022007, 2014.
[22] Mironov SV, Melnikov AS, Buzdin AI. Phys. Rev. Lett. 114:227001, 2015.
[23] Petrashov VT, Antonov VN, Maksimov SV, Shaikhaidarov RS. JETP Lett. 59:523, 1994.
[24] Giroud M, Courtois H, Hasselbach K, Mailly D, Pannetier B. Phys. Rev. B 58:R11872, 1998.
[25] Wang J, Singh M, Tian M, Kumar N, Liu B, Shi C, Jain JK, Samarth N, Mallouk TE, Chan MHW. Nature Physics 6:389, 2010.
[26] Champel T, Löfwander T, Eschrig M. Phys. Rev. Lett. 100:077003, 2008.
[27] Konschelle F, Cayssol J, Buzdin AI. Phys. Rev. B 78:134505, 2008.
[28] Trifunovic L. Phys. Rev. Lett. 107:047001, 2011.
[29] Trifunovic L, Popovic Z, Radovic Z. Pys. Rev. B 84:064511, 2011.
[30] Houzet M, Buzdin A. Phys. Rev. B 76:060504(R), 2007.
[31] Buzdin A. Phys. Rev. Lett. 101:107005, 2008.
[32] Kadigrobov A, Ivanov Z, Claeson T, Shekhter RI, Jonson M. Europhys. Lett. 67:948, 2004.
[33] Beenakker CWJ. Annu. Rev. Con. Mat. Phys. 4:113, 2013.
[34] Alicea J. Rep. Prog. Phys. 75:076501, 2012.
[35] Konschelle F, Cayssol J, Buzdin A. Phys. Rev. B 82:180509, 2010.
[36] Qi X-L, Zhang S-C. Rev. Mod. Phys. 83:1057, 2011.
[37] Castro Neto AH, Guinea F, Peres NMR, Novoselov KS, Geim AK. Rev. Mod. Phys. 81:109, 2009.
[38] Charlier J-C, Blase X, Roche S. Rev. Mod. Phys. 79:677, 2007.
[39] Mourik V, Zuo K, Frolov SM, Plissard SR, Bakkers EPAM, Kouwenhoven LP. Science 336:1003, 2012.
[40] Nikolaeva A, Gitsu D, Konopko L, Graf MJ, Huber TE. Phys. Rev. B 77:075332, 2008.
[41] Churchill HOH, Fatemi V, Grove-Rasmussen K, Deng MT, Caroff P, Xu HQ, Marcus CM. Phys. Rev. B 87:241401(R), 2013.
[42] Hofmann P. Progr. Surf. Sci. 81:191, 2006.
[43] Seradjeh B, Wu J, Phillips P. Phys. Rev. Lett. 103:136803, 2009.
[44] Koroteev YuM, Bihlmayer G, Gayone JE, Chulkov EV, Blugel S, Echenique PM, Hofmann Ph. Phys. Rev. Lett. 93:046403, 2004.

[45] Hirahara T, Miyamoto K, Matsuda I, Kadono T, Kimura A, Nagao T, Bihlmayer G, Chulkov EV, Qiao S, Shimada K, Namatame H, Taniguchi M, Hasegawa S. Phys. Rev. B 76:153305, 2007.
[46] Li C, Kasumov A, Murani A, Sengupta S, Fortuna F, Napolskii K, Koshkodaev D, Tsirlina G, Kasumov Y, Khodos I, Deblock R, Ferrier M, Guéron S, Bouchiat H. Phys. Rev. B 90:245427, 2014.
[47] Beenakker CWJ. Phys. Rev. Lett. 67:3836, 1991.
[48] Rashba EI. Fiz. Tverd. Tela (Leningrad) 2:1224, 1960 [Sov. Phys. Solid State 2:1109, 1960].
[49] Bychkov YuA, Rashba EI. Pis'ma Zh. Eksp. Teor. Fiz. 39:66, 1984 [JETP Lett. 39:78, 1984].
[50] Yokoyama T, Eto M, Nazarov YuV. Phys. Rev. B 89:195407, 2014.
[51] Konschelle F, Tokatly IV, Bergeret FS. Phys. Rev. B 92:125443, 2015.
[52] Schäpers T. Superconductor/Semiconductor Junctions. Springer Tracts on Modern Physics, vol. 174. Springer, Berlin Heidelberg, 2001.
[53] Volkov AF, Magnée PHC, van Wees BJ, Klapwijk TM. Physica C 242:261, 1995.
[54] Fagas G, Tkachov G, Pfund A, Richter K. Phys. Rev. B 71:224510, 2005.
[55] Sau JD, Lutchyn RM, Tewari S. S. Das Sarma, Phys. Rev. B 82:094522, 2010.
[56] Kopnin NB, Melnikov AS. Phys. Rev. B 84:064524, 2011.
[57] Samokhin KV. Phys. Rev. B 70:104521, 2004.
[58] Kaur RP, Agterberg DF, Sigrist M. Phys. Rev. Lett. 94:137002, 2005.
[59] Buzdin AI, Kulić ML. J. Low Temp. Phys. 54:203, 1984.
[60] Gardner HJ, Kumar A, Yu L, Xiong P, Warusawithana MP, Wang L, Vafek O, Schlom DG. Nat. Phys. 7:895, 2011.
[61] Nugent P, Sosnin I, Petrashov VT. J. Phys. Condens. Matter 16:L509, 2004.
[62] Altland A, Simons BD, Taras-Semchuk D. Adv. Phys. 49:321, 2000.
[63] Ostrovsky PM, Skvortsov MA, Feigel'man MV. Phys. Rev. Lett. 87:027002, 2001.
[64] Zyuzin AYu, Spivak B, Hruska M. Europhys. Lett. 62:97, 2003.
[65] Mel'nikov AS, Buzdin AI. Phys. Rev. Lett. 117:077001, 2016.
[66] Al'tshuler BL. Pis'ma Zh. Eksp. Teor. Fiz. 41:530, 1985 [JETP Letters 41:648, 1985].
[67] Lee PA, Stone AD. Phys. Rev. Lett. 55:1622, 1985.
[68] Al'tshuler BL, Spivak BZ. Zh. Eksp. Teor. Fiz. 92:609, 1987 [Sov. Phys. JETP 65:343, 1987].
[69] Chakravarty S, Schmid A. Phys. Rep. 140:193, 1986.
[70] Thouless DJ. Phys. Rev. Lett. 39:1167, 1977.
[71] Robinson JWA, Piano S, Burnell G, Bell C, Blamire MG. Phys. Rev. B 76:094522, 2007.
[72] Champel T, Eschrig M. Phys. Rev. B 72:054523, 2005.
[73] Kompaniiets M, Dobrovolskiy OV, Neetzel C, Porrati F, Brotz J, Ensinger W, Huth M. Appl. Phys. Lett. 104:052603, 2014.
[74] Kompaniiets M, Dobrovolskiy OV, Neetzel C, Ensinger W, Huth M. J. Supercond. Nov. Magn. 28:431, 2015.
[75] Akkermans E, Montambaux G. Mesoscopic Physics of Electrons and phonons, Cambridge Uni. Press, New York, 2007.
[76] Fominov YaV, Golubov AA, Karminskaya TYu, Kupriyanov MYu, Deminov RG, Tagirov LR. Pis'ma v JhETF 91:329, 2010 [JETP Lett. 91:308, 2010].
[77] Mironov SV, Buzdin AI. Phys. Rev. B 89:144505, 2014.